applied sciences

MDPI

Review

Physicochemical Characteristics and Prospects of Carbon Nanomaterials and Composites for Gas Sorption

Nazym Asanbek [1,2], Almagul Kerimkulova [2,3,*], Leticia F. Velasco [4], Aitugan Sabitov [2,5], Meiram Atamanov [2,5], Yersultan Yermoldanov [1,2], Yerlan Doszhanov [1,2] and Guzal Ismailova [1]

1 Faculty of Chemistry and Chemical Technology, Al-Farabi Kazakh National University, Al-Farabi Ave. 71, Almaty 050040, Kazakhstan; naziko-asanbek@mail.ru (N.A.); eursultanermoldanov@gmail.com (Y.Y.); doszhanov_yerlan@mail.ru (Y.D.); guzal2097@gmail.com (G.I.)
2 Institute of Combustion Problems, Bogenbay Batyr 172, Almaty 050012, Kazakhstan; aitugans@mail.ru (A.S.); amk1310@mail.ru (M.A.)
3 Department of Materials Science, Nanotechnology and Engineering Physics, Satbayev University, Satbayev Str., 22a, Almaty 050013, Kazakhstan
4 Department of Chemistry, Royal Military Academy, Avenue de la Renaissance 30, 1000 Brussels, Belgium; leticia.fernandezvelasco@mil.be
5 Faculty of Natural Sciences, Kazakh National Women's Teacher Training University, Gogol Str., 114, k. 1, Almaty 050000, Kazakhstan
* Correspondence: almusha_84@mail.ru

Abstract

This review presents a modern comprehensive analysis of the physicochemical characteristics of carbon materials for the sorption of gases. The main classes of carbon sorbents are considered as follows: nanotubes, activated carbon, graphene, fullerene, composite materials, and organic vapors. Modern methods of modification of carbon materials are systematized. Particular attention is paid to the effect of particle size, morphology, and porous structure on the kinetics and equilibrium characteristics of adsorption. The results of experimental and theoretical studies of the adsorption of the gases (CO_2, SO_2, NO_x, H_2S, NH_3, and CO) are analyzed. A comparative economic analysis of carbon materials is carried out, taking into account the cost of production and estimated costs of modification. Modern areas of application of carbon sorbents are analyzed as follows: industrial gas purification, automotive filters, air conditioning systems, personal protective equipment, and gas sensors. Particular attention is paid to the study of the prospects and future of materials. Prospective development directions are considered, including the creation of hierarchically porous structures, the development of self-healing materials, and integration with artificial intelligence to optimize adsorption processes. The cost of graphene and nanotube production is predicted to decrease by 50–70% by 2030, which will lead to an expansion of their commercial application.

Keywords: carbon adsorbents; nanotubes; graphene; fullerenes; gas capture; adsorption kinetics; surface functionalization; regeneration

Academic Editor: Andrea Atrei

Received: 26 December 2025
Revised: 30 January 2026
Accepted: 2 February 2026
Published: 4 February 2026

1. Introduction

The sorption of gases, including CO, CO_2, N_2O, CH_4, and other industrial emissions, is one of the key tasks of modern environmental and chemical engineering. Carbon monoxide (CO), formed mainly during incomplete combustion of carbon-containing fuels, poses a serious toxicological hazard due to its high affinity for hemoglobin and its ability to cause hypoxic conditions [1,2]. At the same time, the intensive development of the energy,

chemical, and petrochemical industries is accompanied by a steady increase in greenhouse gas emissions, including carbon dioxide (CO_2), nitrous oxide (N_2O), and methane (CH_4), which contribute significantly to global climate change [3].

In the context of stricter environmental regulations and the transition to the concept of sustainable development, carbon nanostructured materials are attracting increasing interest. This class of materials is considered a viable platform for the development of gas purification systems with enhanced efficiency and environmental compatibility. As noted in the article [4], the unique combination of a high specific surface area, a developed porous structure, and the possibility of targeted chemical modification make carbon nanomaterials particularly attractive for trapping and neutralizing toxic and greenhouse gases.

Porous carbon materials are characterized by a high ability to adsorb components of the gas phase and are traditionally considered as one of the most economically feasible adsorbents [5]. Adsorption remains one of the simplest and most energy efficient methods of cleaning gas emissions from toxic and vapor pollutants. However, as Ajmal Z et al. [6] points out, the intensification of technological processes and the increasing complexity of industrial emissions lead to a decrease in the efficiency of traditional adsorption systems. Modern gas streams are multicomponent mixtures containing trace amounts of highly toxic organic compounds, halogen derivatives, and heterocyclic molecules [7–9], for which classical activated carbons and zeolites exhibit limited selectivity and pronounced competitive adsorption.

Additional technological limitations are associated with the need to ensure high mass transfer rates with minimal hydraulic resistance, which narrows the scope of application exclusively for microporous adsorbents. Operation in conditions of elevated temperatures and chemically aggressive environments requires high thermal and chemical stability of materials. At the same time, the concept of industrial ecology assumes not only the removal of pollutants, but also their selective extraction with the possibility of adsorbent regeneration at minimal energy costs [10–14].

In this context, carbon nanomaterials represent a class of adsorbents with a controlled pore structure and flexibly configurable surface chemistry [15–18]. The possibility of targeted defect management, functional groups, and electronic properties opens up new approaches to the development of a new generation of adsorbents combining high capacity, selectivity, and regenerability for gas purification and capture of valuable components from industrial emissions [19–22].

The relevance of carbon nanomaterials is determined by the need for modern, highly efficient adsorbents for modern gas purification systems, digitalization of chemical industries, and the implementation of carbon capture technologies as part of the global energy transition.

The purpose of this article is to analyze the adsorption properties of carbon materials of various structures (nanotubes, activated carbon, graphene, fullerenes, and composite materials) for gas sorption with an assessment of the prospects for their use and determining the future of these materials.

Studies were included if they addressed the use of carbon-based materials, such as activated carbons, carbon nanotubes, graphene, and their composites, for the adsorption of toxic gases. The focus was on adsorption capacity, kinetics, regeneration, and techno-economic or environmental assessment. Only peer-reviewed journal articles in English published between 2016 and 2025 were considered.

A literature search was conducted in Scopus, Web of Science, ScienceDirect, and Google Scholar. Relevant references cited in key articles were also manually screened to identify additional sources.

Data were extracted manually, and any missing or unclear summary statistics were marked as "not presented". The extracted information was compiled into structured tables and visualized using diagrams to summarize material properties, adsorption performance, and application areas.

Research issues:

1. What are the structural features of various types of carbon materials (nanotubes, graphene, fullerenes, and activated carbon) that determine their selectivity for specific classes of gases?
2. How do the methods of surface functionalization of carbon nanomaterials affect the adsorption efficiency of various toxicants and the possibility of adsorbent regeneration?
3. What synergistic effects are observed in composite carbon materials, and how do these effects affect the overall adsorption capacity and adsorption kinetics in gas purification processes?
4. Which technological limitations hinder the integration of carbon nanomaterials into industrial gas purification systems, and which approaches may enable their mitigation?
5. What are the prospects for the development of carbon adsorbents in the context of creating intelligent gas purification systems and implementing the principles of circular economy in the chemical industry?

2. Carbon Nanotubes: Structure, Surface Chemistry, and Mechanisms of Gas Adsorption

2.1. Chirality and Morphology of CNTs

Carbon nanotubes (CNTs) are cylindrical sp^2-hybridized structures with a diameter of 0.4–100 nm and a length/diameter ratio of 10^3–10^4 [23]. Single-walled nanotubes are characterized by a diameter of 0.4–2.0 nm [24] and a specific surface area of up to 2600 m^2/g, while multi-walled nanotubes have a diameter of 2–100 nm and a surface area of 100–500 m^2/g. Chirality determines the electronic properties and reactivity of the surface [25].

Figure 1 illustrates the fundamental relationship between the idealized structural description of carbon nanotubes and their experimentally observed morphology. Figure 1a summarizes the crystallographic basis of CNT formation based on the folding of a graphene sheet along the chirality vector (n,m), which determines the nanotube diameter, chiral angle, and atomic configuration. The difference between the armchair, zigzag, and chiral structures emphasizes the intrinsic relationship of geometry with the electronic structure, since it is these parameters that determine the symmetry of electronic states and determine the metallic or semiconductor nature of conductivity. In multi-wall and double-wall CNTs, the coexistence of coaxial shells with different chiral indices leads to additional complexity due to inter-wall van der Waals interactions and electronic coupling, which leads to a modification of the band structure and transport properties compared with single-layer nanotubes.

Figure 1b presents characteristic high-resolution electron microscopy images demonstrating the deviation of real CNTs from idealized structural models. The observed bends, diameter fluctuations, wall distortions, and local defects reflect the kinetic nature of nanotube growth and the influence of synthesis conditions, including catalyst composition and temperature gradients. Such structural imperfections play a dual role: on the one hand, the reduction in long-range order and charge carrier mobility may occur, while on the other hand, the formation of chemically active centers critically important for adsorption, functionalization, and catalytic processes is promoted. As a result, the functional characteristics of CNT-based materials are determined not only by nominal chirality, but also by the interaction between the degree of structural order, defect density, and hierarchical morphology.

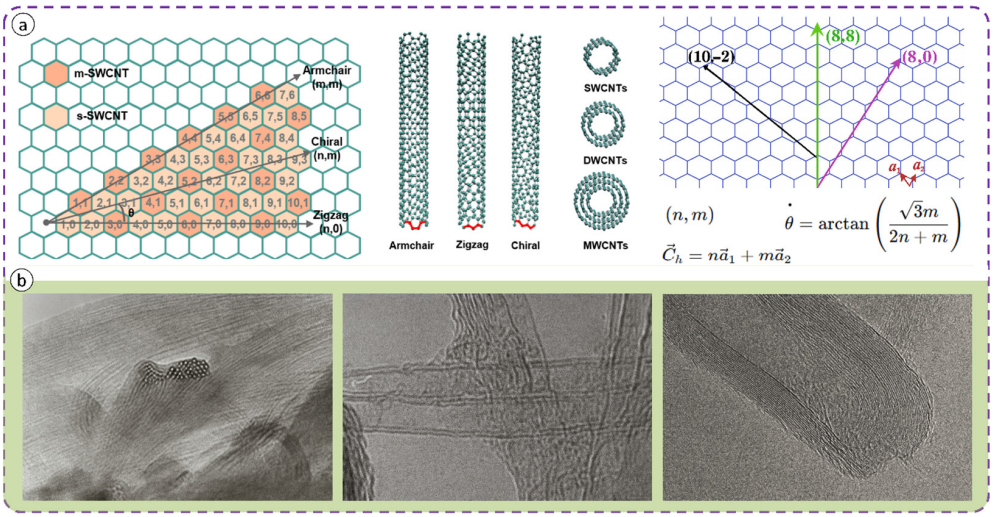

Figure 1. The structure and morphology of carbon nanotubes: (**a**) a diagram of the chirality and types of CNTs formed during the folding of a graphene sheet [26,27]; (**b**) characteristic electron microscopic images demonstrating the actual morphology and defects of nanotubes [28].

2.2. Defects and Functionalization of the Surface

CNTs have unique sorption characteristics that depend on purity, defectiveness, porosity, specific surface area, number of functional groups, and density of active centers [29]. Their hollow structures, high concentration of specific surface areas, and the presence of oxygen- and nitrogen-containing functional groups (–COOH, –OH, and $–NH_2$) make CNTs an almost perfect sorption material for removing organic and inorganic pollutants. The main driving forces of adsorption are π-π interactions, hydrophobic interactions, electrostatic interactions, and charge transfer [30,31]. The special properties of CNTs, including their high mechanical strength, thermal and chemical stability, as well as the possibility of chemical modification, make them ideal candidates for use in gas purification processes [32]. The hollow tubular structure of CNTs creates additional adsorption centers on both the outer and inner surfaces of nanotubes, which significantly increases their adsorption capacity compared to traditional carbon materials [33].

Pristine carbon nanotubes exhibit several limitations, including weak interactions with many solvents and a limited density of surface functional groups for metal ion attachment. Oxidative treatment overcomes these limitations by increasing the concentration of hydroxyl, carboxyl, and carbonyl groups on the surface, enhancing solubility in aqueous media, and generating chemically bound oxygen-containing functionalities [34].

The CNT diameter is less than 1 nm [35], which provides a molecular sieve effect with selectivity for the kinetic diameters of molecules. The optimal diameter for the maximum adsorption capacity is 1.5–3.0 nm. Structural defects create active centers with binding energy 20–50% higher than defect-free surfaces at an optimal defect concentration of 1–5%. Defects in the structure of carbon nanotubes increase their adsorption and catalytic properties, creating active centers with binding energy 20–50% higher than defect-free surfaces. At an optimal defect concentration of 1–5%, the adsorption capacity increases, selectivity to certain gas molecules improves, and catalytic activity increases due to the appearance of preferred adsorption centers and new reaction pathways. Exceeding the optimal defect concentration can lead to degradation of the CNT structure and a decrease in their mechanical strength; therefore, the controlled introduction of defects is a key factor for maximizing the effectiveness of CNTs in gas purification applications [36,37].

Oxidative functionalization of HNO_3/H_2SO_4 introduces carboxyl, hydroxyl, and carbonyl groups with a concentration of 1.5–4.5 mmol/g. While O_2-plasma selectively creates

oxygen groups, N_2-plasma introduces various forms of nitrogen in a ratio of 3:2:1. Cu-modification provides selective adsorption of H_2S at an optimal load of 8–12 wt.%, and Ni-activation increases the capacity of NH_3 by 3–4 times. N-doping creates the main centers effective for the adsorption of SO_2 and CO_2 at a nitrogen concentration of 3–8 at.%. The kinetics of adsorption is described by a pseudo-second-order model with rate constants 0.05–0.12 mg/(g·min) for various gases. The isotherms correspond to the Langmuir model with maximum capacities of SO_2 45–120 mg/g, NO_2 35–85 mg/g, NH_3 25–70 mg/g, and H_2S 15 15–180 mg/g. The selectivity coefficients reach SO_2/N_2 = 150–450 and NO_2/NO = 10–25 for functionalized samples [38]. Thermal regeneration at 150–250 °C restores 95–98% of the adsorption capacity with a loss of no more than 5–15% after 500 cycles. CVD synthesis provides a productivity of 10–50 g/h at a cost of 50–200 USD·kg^{-1}, and economic efficiency is achieved with a capacity of more than 50 mg/g and a service life of over 2 years [39].

2.3. Mechanisms of Gas Adsorption

The mechanisms of gas adsorption on carbon nanotubes are characterized by pronounced diversity and depend on the nature of the adsorbed molecule, the surface condition, and the type of CNT modification.

Figure 2 illustrates the variety of mechanisms of interaction between gas molecules and carbon nanotubes, demonstrating that the high sorption efficiency of CNT is due not to a single process, but to a combination of physical adsorption, chemisorption, and surface-mediated reactions. This multi-mechanisticity reflects the structural and chemical flexibility of the carbon matrix, as well as its ability to adapt to the nature of the adsorbed gas.

The physical adsorption of CO_2 on the CNT surface is mainly determined by dispersion van der Waals interactions and π-π conjugation with a graphite-like surface [40]. Despite the relatively weak nature of these interactions, the high specific surface area, the developed curvature of the walls, and the presence of defects contribute to an increase in the density of adsorbed molecules [41]. This mechanism is reversible and energetically advantageous, which makes CNTs promising materials for cyclic CO_2 capture processes.

Carbon dioxide is one of the most studied gases in the context of adsorption on CNTs. Studies show [32] that CO_2 adsorption on CNTs is primarily a physical process characterized by an exothermic nature. At a temperature of 25 °C and a pressure of 10 bar, the maximum CO_2 adsorption can reach 9.57 mmol/g for unmodified CNTs. However, modification of CNTs with catalysts such as Fe-Ni/AC significantly improves the adsorption characteristics, allowing an adsorption capacity of up to 424.1 mg/g to be achieved under the same conditions. The temperature dependence of CO_2 adsorption demonstrates the characteristic behavior of physisorption: with increasing temperature, the adsorption capacity decreases due to increased molecular motion and weakening of intermolecular interactions. At low pressures, CO_2 molecules are preferentially adsorbed inside nanotubes to form a monolayer, which is due to the stronger potential for solid–fluid interaction in the confined space of the tube.

The interaction of NH_3 with CNT, on the contrary, is characterized by a pronounced chemisorption contribution. Oxygen-containing functional groups and defective surface areas act as acid centers, providing donor-acceptor interactions and the formation of hydrogen bonds. This leads to a stronger fixation of ammonia molecules and explains the high selectivity of CNT with respect to polar and base gases. At the same time, the degree of surface functionalization is a key factor determining the balance between the capacity and reversibility of adsorption [42,43]. High affinity for CNTs increases on the surface of modified nanotubes, which is due to the possibility of increasing the number of hydrogen bonds with oxygen-containing functional groups [44]. The equilibrium amount

of ammonia adsorption varies from 22.69 to 90.05 mg/g CNT, depending on temperature and pressure, which confirms the potential of CNTs as effective adsorbents for this toxic gas.

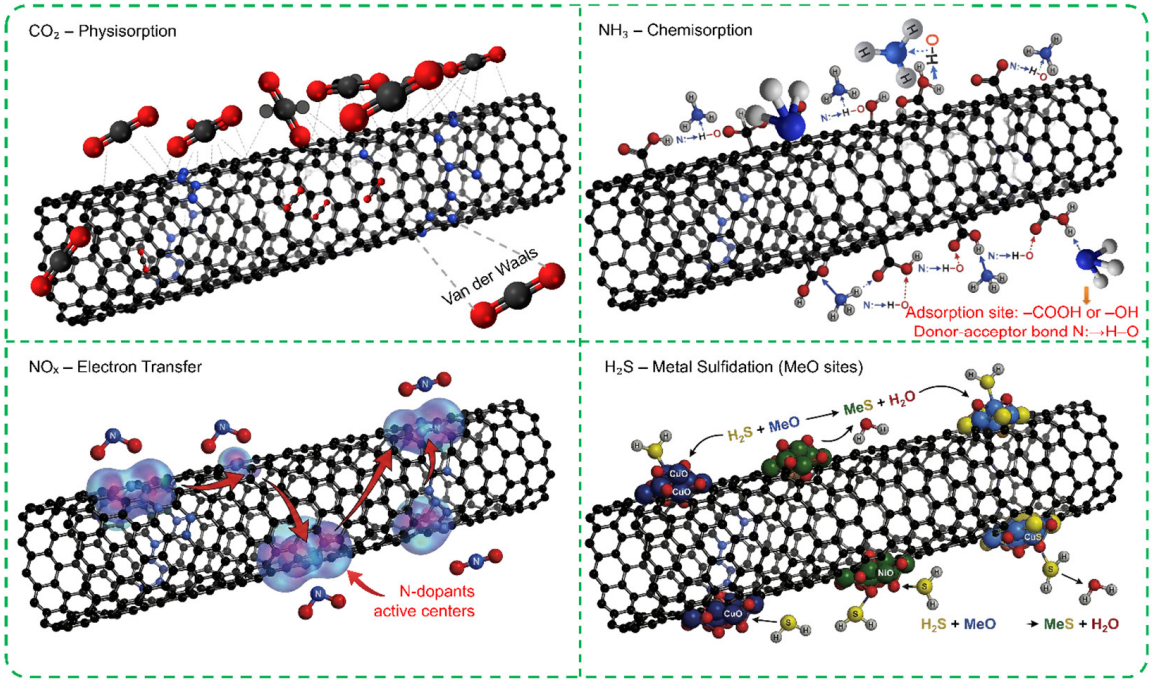

Figure 2. Schematic representation of the main mechanisms involved in gas adsorption on carbon nanotubes. These mechanisms include physical adsorption of CO_2, chemisorption of NH_3 on functional groups on the surface, charge transfer through interaction with NO_x, and metal-mediated adsorption of H_2S on modified CNTs (the conceptual scheme shown in this figure has been adapted and scientifically redesigned by the CorelDRAW Graphics Suite 2021 application based on the graphic style and structural principles illustrated in the reference information) [45].

Hydrogen sulfide (H_2S) and sulfur dioxide (SO_2) are of particular interest due to their high toxicity and corrosive activity. Traditional methods of their removal often face problems with equipment corrosion and low efficiency at low concentrations [45]. CNTs show promising results for the adsorption of sulfur-containing gases, especially when their surface is modified by specific functional groups [46]. The adsorption of H_2S on CNTs modified with metal or metal oxide nanoparticles is accompanied by surface reactions with the formation of sulfide phases. In this case, CNTs act not only as a carrier, but also as a conducting platform providing efficient electron transfer between active centers and the carbon matrix. This mechanism refers to chemically irreversible or quasi-irreversible processes and provides high sorption capacity and selectivity with respect to sulfur-containing gases.

Nitrogen oxides (NO_x) and carbon monoxide (CO) are efficiently adsorbed on CNTs modified with metal catalysts such as nickel. Nickel contributes not only to the adsorption, but also to the catalytic reduction in NO_x to less harmful compounds, as well as the oxidation of CO to CO_2, which significantly increases the efficiency of gas purification. For nitrogen oxides, charge transfer between NO_x molecules and the electronically modified CNT surface plays a crucial role. Doping with heteroatoms, in particular nitrogen, forms local electron-active centers that promote the activation of adsorbed molecules and the stabilization of charge-transfer complexes. Such interactions go beyond classical physical adsorption and explain the high sensitivity of CNT to NO_x, which is of fundamental importance for gas sensors and catalytic applications.

There are various modification methods: application of a polymer matrix of nanoscale metal particles, chemical treatment at high temperatures, and variation of the porous structure for molecular sorption based on the sieve effect [47,48]. An increase in the active surface due to the introduction of CNTs with unique physical and mechanical characteristics makes it possible to increase the sorption capacity. According to Popova A.A. and Shubin I.N., an alternative method involves the preparation of a multicomponent mixture of zeolite, binder, and carbon nanotubes, followed by molding and subsequent heat treatment. The use of a mixture of CaA and NaX zeolites with a binder content of 20–30% and CNM 2–2.5% was experimentally established [49].

Researchers Mollaamin, F.; Monajjemi, M. [19] used theoretical density functional modeling (DFT) to study the effect of toxic gases on the electronic properties of zigzag graphene nanotubes (GNTs). It has been established that formaldehyde and hydrogen sulfide are weakly physisorbed on the surface of graphene nanotubes. In this case, charge is transferred from the molecules to the nanotubes. As noted by Buzaeva M. V. et al. [50], the key problem of the practical application of CNTs is their high ability to agglomerate, which makes it difficult to introduce the material into the matrix. Carbon nanotubes are becoming increasingly common in sorption processes for cleaning contaminated solutions and process fluids.

The oxidative acid treatment of multi-walled carbon nanotubes (MWCNTs) was studied by treating MWCNTs with HNO_3 and a mixture of H_2SO_4/HNO_3 in a 3:1 ratio. The preliminary acid treatment of MWCNTs was performed to achieve two goals: (1) removal of metal catalyst particles from the initial MWCNTs and (2) carboxylation of MWCNTs to introduce carboxyl groups onto the surface of MWCNTs before amino functionalization. Treatment with 15M HNO_3 ensures the formation of 5.2 at.% of surface oxygen with a mass loss of only 6.8%, while treatment with 10M H_2SO_4/HNO_3 yields 3.2 at.% oxidation with a mass loss of about 17% [51].

Collectively, the presented mechanisms demonstrate that carbon nanotubes are a universal platform for gas adsorption, the properties of which can be purposefully adapted by controlling the structure, defects, and surface chemistry.

3. Activated Carbons: Structure, Activation Methods, and Mechanisms of Gas Adsorption

Activated carbon is a highly porous carbon material obtained by thermal or chemical activation of various carbon-containing precursors [52,53]. Activated carbon is an amorphous carbon matrix with a developed porous structure characterized by a specific surface area of 500–3000 m^2/g and a total pore volume of 0.3–2.0 cm^3/g [54].

The structure consists of graphite microcrystallites 1–3 nm in size, separated by pores: micropores (<2 nm), mesopores (2–50 nm), and macropores (>50 nm) in a ratio of 60–80:15–25:5–15%, respectively.

The chemical composition includes 85–98% carbon, and 0.5–8% oxygen with oxygen-containing functional groups with a density of 0.5–5.0 mmol/g. Physical adsorption dominates for nonpolar molecules in micropores through dispersion interactions with an energy of 8–25 kJ/mol according to the Dubinin–Radushkevich volume filling mechanism. Chemisorption occurs on functional groups with a binding energy of 40–200 kJ/mol [55,56].

Micropores provide 70–90% of the adsorption capacity due to the effect of overlapping adsorption potentials. The optimal micropore sizes for the adsorption of the following gases are SO_2—0.6–0.8 nm, H_2S—0.5–0.7 nm, and NH_3—0.4–0.6 nm. A narrow distribution of micropores (0.5–1.2 nm) with a coefficient of inhomogeneity, W_0/W_1 = 1.2–2.0, ensures maximum volumetric capacity.

3.1. Formation of Porous Structure: Chemical and Physical Activation

The activation method is a key factor determining the morphology, pore distribution, and chemical state of the activated carbon surface.

Schematic representation (Figure 3) of an integrated technological route for producing activated carbon with a high specific surface area from biomass. The process includes a stage of carbonation of the initial biomass feedstock in an inert atmosphere (N_2) at 550 °C with a controlled heating rate, subsequent physical mixing of the carbonate with a chemical activator and a stage of chemical activation at 850 °C in an inert medium (Ar), followed by washing with deionized water to a neutral pH and drying. Alternatively or additionally, physical activation in the CO_2 stream at 750 °C is realized, ensuring the development of a porous structure. The combination of chemical and physical activation makes it possible to significantly reduce the total process time and obtain activated carbon with a high specific surface area and developed micro- and mesoporosity.

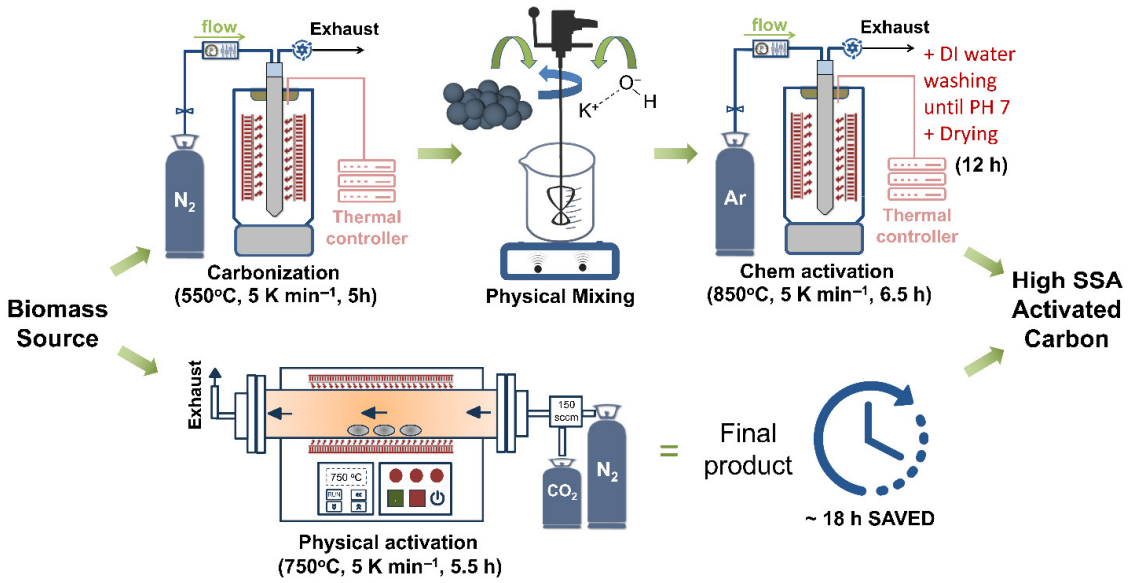

Figure 3. Technological scheme for the production of highly porous activated carbon from biomass using carbonation and combined chemical and physical activation [54].

Table 1 summarizes the main strategies for activated carbon activation and modification. Physical activation using CO_2 vapor develops micropores and ensures physisorption of small molecules at high temperatures (800–1000 °C). Chemical activation with $ZnCl_2$, H_3PO_4, or KOH produces ultra-micropores, high adsorption capacity, and enhanced selectivity. Oxidative functionalization introduces oxygen-containing groups (–COOH, –OH, –C=O), improving adsorption of basic gases. Nitrogen doping and metal modification allow for tuning adsorption properties for acidic gases or specific toxic gases (H_2S and SO_2). These examples illustrate how activation conditions influence the structural and functional characteristics of activated carbons.

Figure 4 shows the fundamental difference in the formation of the porous structure of activated carbon during chemical and physical activation. Chemical activation with potassium hydroxide at 850 °C leads to the intensive development of micro- and ultramicroporosity, accompanied by the formation of cracks and a high density of active centers, whereas physical activation in the atmosphere of CO_2 at 750 °C mainly contributes to the formation of mesopores and an increase in the available specific surface area of the carbon matrix.

Table 1. Key strategies for activated carbon activation and modification.

Approach	Conditions/Modifier	Structural Characteristics	Adsorption Effects	Temperature/ Conditions	Ref.
Physical activation	Vapor, CO_2	SSA 800–2000 m^2/g; micropores	Physisorption of small molecules	800–1000 °C	[57]
Chemical activation	$ZnCl_2$, H_3PO_4, KOH	SSA 1000–3500 m^2/g; ultra-micropores	High adsorption capacity and selectivity	KOH:C = 3–4:1	[57]
Oxidative functionalization	HNO_3	–COOH, –OH, –C=O	Increased adsorption of basic gases × 2–5	Liquid-phase treatment	[57]
Nitrogen doping	NH_3	N 1–5 at.%	Enhanced adsorption of acidic gases	600–900 °C	[58]
Metal modification	Cu, Fe	Me/MeO center	Selective adsorption of H_2S and SO_2	5–20 wt.%	[59]

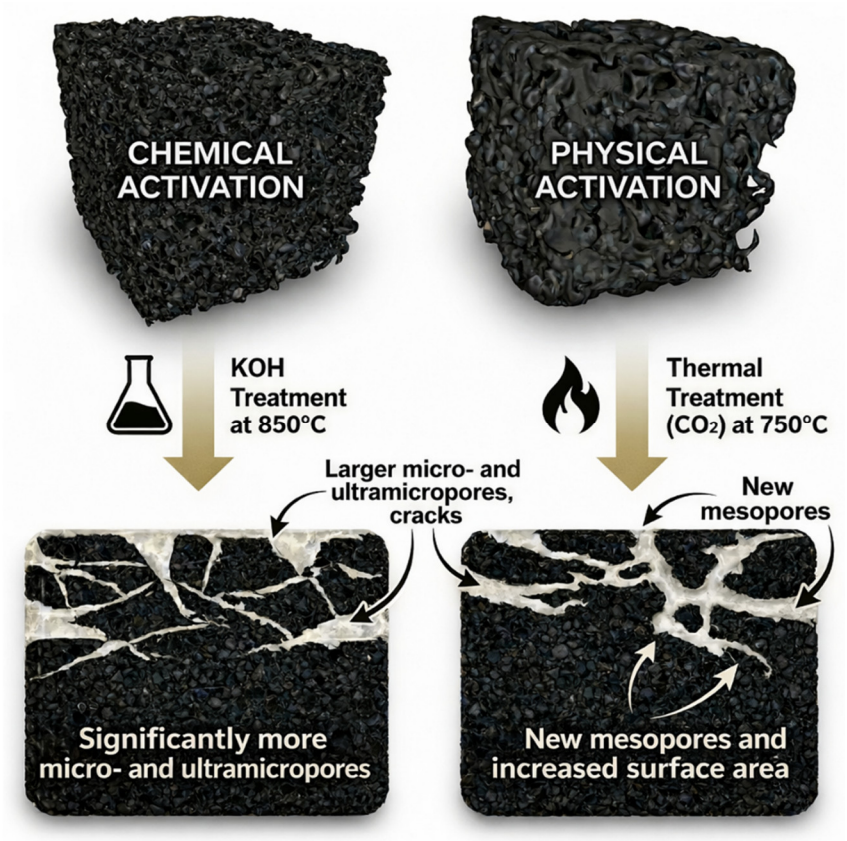

Figure 4. Comparison of chemical (KOH) and physical (CO_2) activation of activated carbon and their effect on the formation of a porous structure [54].

3.2. Surface Chemistry and Defects of Activated Carbons

The surface chemistry of activated carbon is formed both during activation and during subsequent modifications. Oxygen-containing functional groups (carboxylic, phenolic, lactone, and carbonyl) are introduced during acid treatment or oxidation and form acid-base centers with a density of up to several mmol/g. Nitrogen alloying, carried out by heat treatment in an NH_3 atmosphere or using nitrogen-containing precursors, creates electron-active centers of pyridine, pyrrole, and graphite-like types.

Figure 5 shows a set of experimental data demonstrating the effect of the activation method on the morphology, porous structure, and structural ordering of activated carbons. The SEM images (a, b) show significant differences in the micromorphology of the samples obtained by chemical (KOH) and physical (CO_2) activation, reflecting the different nature

of the porous structure development. The analysis of the pore distribution (c, d) indicates the dominance of micropores during chemical activation and a more pronounced contribution of mesopores in the case of physical activation, which determines the differences in adsorption behavior.

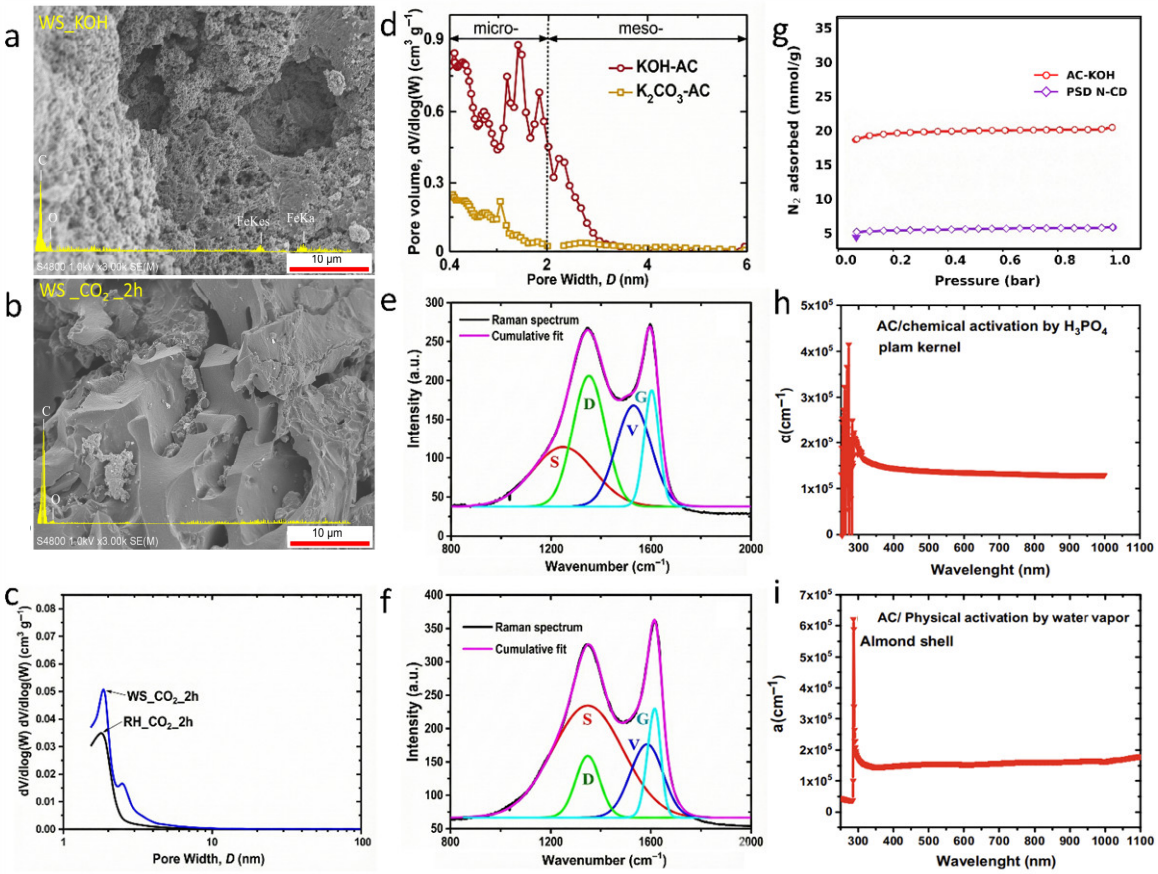

Figure 5. Structural and adsorption characteristics of activated carbons obtained by chemical and physical activation: (**a**,**b**) SEM images [60]; (**c**,**d**) pore size distribution [61]; (**e**,**f**) decomposition of Raman spectra [62]; (**g**) isotherms of N_2 adsorption [62]; and (**h**,**i**) optical spectra of samples obtained by various activation methods [63].

As follows from the Raman analysis (Figure 5e,f), an increase in defects is accompanied by an increase in the ID/IG ratio, reflecting an increase in the proportion of disordered sp^2 regions. These defects should not be considered undesirable, as the presence of defects increases surface reactivity, enhances chemisorption interactions, and enables the anchoring of metal nanoparticles.

3.3. Mechanisms of Gas Adsorption in Activated Carbons

The variety of mechanisms of gas adsorption on activated carbon is clearly summarized in Figure 6, where it is shown that sorption processes are determined by a combination of volumetric filling of micropores, surface physico-chemical interactions and capillary effects.

The adsorption of CO_2 on activated carbon occurs mainly through a physical mechanism, while the efficiency of the process strongly depends on the pore structure and process conditions. Studies show that micropores with a diameter of 0.5–0.9 nm provide optimal CO_2 adsorption due to the strong interaction of gas molecules with the pore walls [64]. The adsorption capacity of activated carbon for CO_2 at atmospheric pressure and 25 °C is usually 1.5–4.0 mmol/g, which depends on the specific surface area, volume

of micropores and surface chemistry. The Langmuir model well describes the isotherms of CO_2 adsorption on activated carbon with a correlation coefficient of about 0.99, which indicates predominantly monomolecular adsorption. Chemical modification of activated carbon with amino-containing compounds significantly improves its ability to capture CO_2. Impregnation with monoethanolamine, diethanolamine, or polyethylenamine creates chemisorption centers capable of binding CO_2 to form carbamates and bicarbonates. Such modified coals can reach an adsorption capacity of 3–6 mmol/g at low concentrations of CO_2, which makes them attractive for post-combustion carbon dioxide capture [65].

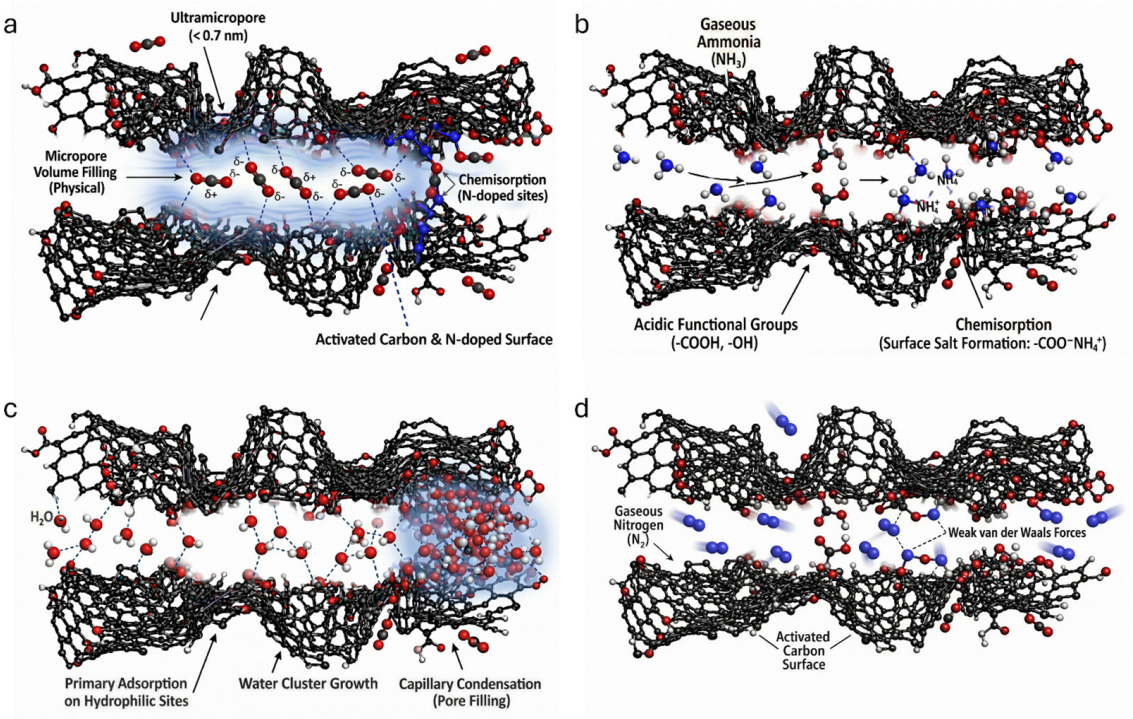

Figure 6. Schematic visualization of the mechanisms of adsorption of gases and vapors in the pores of activated carbon: (**a**) filling of ultra- and micropores and chemisorption on N-doped centers; (**b**) chemisorption of NH_3 on acidic functional groups; (**c**) adsorption of H_2O with cluster formation and capillary condensation; and (**d**) weak physical adsorption of N_2 due to van der Waals interactions. The proposed adsorption mechanism was inspired by the work of Vega et al. [66].

Chemical adsorption (chemisorption) involves the formation of chemical bonds between adsorbed molecules and active centers on the surface of coal. Chemisorption is characterized by higher enthalpies (40–200 kJ/mol), specificity to certain types of molecules, and often irreversibility of the process. To enhance chemical adsorption, activated carbon is often impregnated with various chemical compounds, creating specific active centers for interaction with target gases. Catalytic adsorption is a special case where activated carbon not only adsorbs gases, but also catalyzes their conversion into less toxic or more easily removable compounds. This mechanism is especially important for the removal of gases such as H_2S and NO_x, which can oxidize on the surface of coal to form stable products [67,68].

The adsorption of H_2S on activated carbon occurs through a complex mechanism involving both physical and chemical adsorption. Physical adsorption of H_2S proceeds relatively slowly and occurs mainly in the internal pores of coal, while chemical adsorption proceeds rapidly on the surface of coal [69]. The maximum adsorption capacity of activated carbon for H_2S can reach 164–190 mg/g, depending on the type of coal and the process conditions. The alkaline modification of activated carbon significantly improves its ability to remove H_2S by creating basic centers capable of neutralizing acid gas. Impregnation

with copper, zinc, or iron provides the catalytic oxidation of H_2S to elemental sulfur or sulfates, which increases the total capacity of the adsorbent [70].

SO_2 adsorption is characterized by high affinity to the surface of activated carbon and can occur by both physical and chemical mechanisms. At low concentrations of SO_2 (0.25–9 ppm), the adsorption isotherm is best described by the Sips model [71], which indicates the heterogeneity of the adsorption centers. Humidity significantly affects the adsorption of SO_2: an increase in relative humidity from 25% to 75% leads to a 20-fold increase in the adsorption capacity due to the formation of sulfuric acid.

The adsorption of NH_3 on activated carbon occurs mainly through acid-base interactions with acidic functional groups on the surface of coal. Modification of activated carbon with sulfuric acid or phosphoric acid creates additional acid centers, significantly increasing the adsorption capacity of ammonia. Experimental data show that copper-impregnated activated carbon can reach an adsorption capacity of 1.45 mmol/g NH_3 at room temperature [72]. Bimetallic modification of activated carbon with chlorides and metal oxides ensures effective simultaneous removal of NH_3 and H_2S with high selectivity. The isotherm of NH_3 adsorption is best described by the Langmuir model, and the kinetics follows the pseudo-second-order model [69].

Removal of nitrogen oxides (NO and NO_2) is particularly difficult due to the low reactivity of NO under normal conditions. The presence of oxygen dramatically changes the situation: NO can be oxidized to NO_2 on the surface of activated carbon, which leads to the coadsorption of NO/NO_2. The catalytic oxidation of NO on activated carbon is significantly enhanced at low temperatures, which leads to an extraordinary increase in the adsorption capacity from 3.8 mg/g at 80 °C to 169.1 mg/g at −20 °C [73,74]. Ni-activated carbon composites show high efficiency of CO removal (94.87%) at the exhaust gas temperature of diesel engines. The mechanism involves the adsorption of CO on metal centers, followed by catalytic oxidation with atmospheric oxygen [75].

Figure 7 shows the kinetic dependences of the adsorption of various gases on activated carbons obtained by various methods of activation and surface modification. Typical breakthrough dynamics are shown for H_2S (a), reflecting the gradual saturation of active centers and the high sorption efficiency of KOH-activated carbon. The adsorption of SO_2 on commercial activated carbon (b) is characterized by a rapid increase in capacity at the initial stage, followed by a plateau, while the rate of adsorption naturally decreases as the porous structure is filled.

A comparison of the kinetics of NO_2 (c) adsorption demonstrates the advantage of KOH-activated carbon over HNO_3-modified carbon, which indicates a more favorable combination of porous structure and surface chemistry. The adsorption of CO_2 on KOH-activated carbon (d) proceeds rapidly and reaches a high equilibrium capacity, which indicates the dominant contribution of microporosity and physical adsorption. Taken together, the presented data confirm the key role of the activation and chemical modification method in controlling the kinetics and adsorption capacity of gases.

Considering the modification of activated carbon, it should be noted that activated carbon is obtained from various carbon-containing materials, including wood, coal, coconut shell, peat, and agricultural waste. Physical activation includes carbonation of the starting material at 400–600 °C, followed by activation in an atmosphere of vapor or carbon dioxide at 800–1000 °C [76]. Chemical activation uses chemical reagents (H_3PO_4, KOH, and $ZnCl_2$) to simultaneously carbonize and activate at lower temperatures.

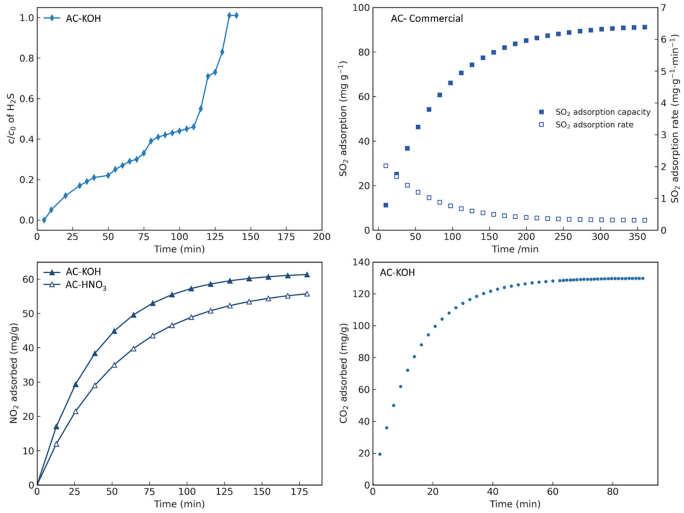

Figure 7. Kinetics of adsorption of H_2S, SO_2, NO_2, and CO_2 on activated carbons with various methods of activation and surface modification [77,78].

An experimental study demonstrates that modification of activated carbon with a solution of NaOH significantly improves the adsorption capacity of the material. NaOH treatment induces the formation of oxygen-containing functional groups on the surface, which can effectively bind to HCl gas molecules. Functionalized activated carbons (FAC) are prepared with various types of alkaline treatment applied to the granular activated carbons precursor [79], including treatment with ammonia, sodium hydroxide, and potassium hydroxide.

The choice of the activation method critically affects the pore structure and the adsorption properties of the resulting coal. Activation with potassium hydroxide provides higher specific surface area and larger pore sizes compared to activation with sulfuric acid. CO_2 activation at high temperatures promotes the development of a microporous structure optimal for the adsorption of small gas molecules. Combined modification methods, including chemical and physical activation, make it possible to obtain coals with optimized properties for specific applications [80].

A study by Lin Y. et al. [81] showed that adsorption on activated carbon H_2S formation of various sulfur-containing products (elemental sulfur S_8, H_2SO_3, and H_2SO_4), which has effect on coal consumption during regeneration: elemental sulfur is desorbed at ~380 °C, almost without damaging carbon structure and reducing chemical consumption of coal 59.8% compared with H_2SO_4, which decomposes with the destruction of the C=C bond, highlighting SO_2, CO_2, and CO, and significantly reducing the strength of the coal, whereas H_2SO_3 removed without the expense of coal. The main contribution to coal consumption is made by the processes of regeneration of sulfur-containing products (more than two thirds of the total consumption), while the decomposition of oxygen groups plays a lesser role, while elemental sulfur is preferable, since it minimizes damage to the carbon frame.

Spiridonova E. A. et al. [82] claim that the efficiency of gas purification can be improved by creating combined adsorption systems based on modified activated carbon. Modification of activated carbon SKT-6 by ultrasonic treatment followed by impregnation with a fullerene solution and thermal fixation leads to a significant increase in the adsorption space, increased hydrophobicity and dynamic activity of the sorbent. Fullerenes on the surface of activated carbon provide improved sorption characteristics for operation in extreme conditions when cleaning gas streams from combustion products, including benzene, n-decane, hydrogen chloride, hydrogen fluoride, nitrogen dioxide, sulfur dioxide, and other toxic compounds. Combined systems, including modified activated carbon and spe-

cialized chemosorbents, demonstrate synergistic effects in the removal of multicomponent gas pollutants [83].

4. Adsorption Properties of Graphene and Its Derivatives: Mechanisms, Modifications, and Applications in Gas Purification

Graphene and its derivatives have attracted considerable attention due to their unique two-dimensional sp^2-hybridized structure, high specific surface area, and exceptional electronic properties. Monolayer graphene is characterized by a thickness of about 0.335 nm and a theoretical specific surface area of up to 2630 m^2/g, whereas experimentally achievable values for real samples are 500–2500 m^2/g, depending on the synthesis method and degree of aggregation. The electronic structure of graphene with a zero band gap and high mobility of charge carriers determines its high sensitivity to adsorption of gas molecules, especially in sensor applications [84]. The electronic structure is characterized by a zero band gap, a charge carrier mobility of up to 15,000 $cm^2/(V \cdot s)$, and a conductivity of 10^6 Cm/m.

4.1. Mechanisms of Gas Adsorption on Graphene

The adsorption of gases on pure graphene in most cases proceeds by the mechanism of physisorption and is determined by dispersion van der Waals interactions with a binding energy of the order of 8–20 kJ/mol. The adsorbed molecules are localized within nanometer regions of the surface with a characteristic lifetime of 10^{-9}–10^{-6} s. Despite the relatively low binding energy, the adsorption of donor and acceptor molecules leads to a noticeable change in the concentration of charge carriers (10^{12}–10^{13} cm^{-2}), which underlies the operation of graphene gas sensors [85].

Figure 8 schematically shows the main mechanisms of gas adsorption on the surface of graphene and N-doped graphene structures, reflecting the role of the electronic structure and local surface chemistry in the formation of sorption properties.

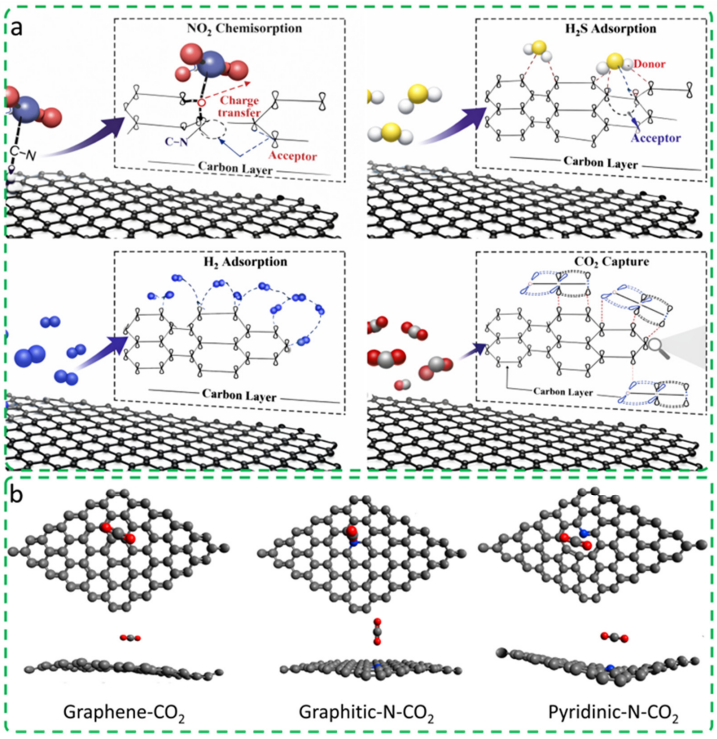

Figure 8. Gas adsorption mechanisms on graphene-based materials: (**a**) schematic illustration of physical adsorption and chemisorption of NO_2, H_2S, H_2, and CO_2 on graphene and N-doped graphene

surfaces, involving donor–acceptor interactions and charge transfer. The panel is a reprinted version of the original figure from Ref. [86]. (**b**) Atomistic models of CO_2 adsorption on pristine graphene as well as graphitic-N and pyridinic-N doped graphene, highlighting the effect of nitrogen configuration on adsorption behavior. Reprinted version of the original figure from Ref. [87].

For NO_2, a predominantly chemisorption mechanism is shown, accompanied by a pronounced charge transfer from the graphene matrix to the adsorbate molecule acting as a strong electron acceptor. The formation of local C–N bonds and the redistribution of electron density in the carbon layer lead to a significant modulation of the electronic properties of graphene, which explains its high sensitivity to NO_2 in sensor and sorption applications. NO_2 demonstrates an adsorption energy of 18–25 kJ/mol with a capacity of 15–40 mg/g and a response time of less than 1 min. NH_3 shows a binding energy of 12–18 kJ/mol with a capacity of 8–25 mg/g with a resistance change of up to 12% at 1 ppm. SO_2 interacts with an energy of 10–15 kJ/mol on pure graphene, increasing to 25–40 kJ/mol on functionalized samples with a capacity of 20–60 mg/g. H_2S demonstrates an energy of 8–12 kJ/mol, increasing to 50–120 mg/g upon metallic activation.

Nitrogen monoxide (NO) is characterized by low polarity and weak adsorption ability on most materials at room temperature. However, the presence of oxygen dramatically changes the situation, since NO can be oxidized to more active nitrogen dioxide (NO_2), which demonstrates a significantly higher adsorption capacity [88].

H_2S adsorption is realized through donor-acceptor interactions, in which the hydrogen sulfide molecule acts as a weak electron donor, and defective or heteroatom-doped modified sections of graphene function as acceptor centers. This mechanism is characterized by a moderate binding energy and a pronounced dependence on the type of functional groups and the degree of surface doping. For molecular hydrogen, a physisorption mechanism is shown due to weak van der Waals interactions, which leads to low adsorption energies and high reversibility of the process. Modification of adsorbents with metals such as copper, zinc, or iron significantly enhances their ability to remove H_2S due to catalytic reactions [89]. The adsorption of NH_3 occurs mainly by the mechanism of acid-base interaction, while materials with a developed system of acidic functional groups are the most effective [78]. Bimodal modification of adsorbents makes it possible to achieve simultaneous effective removal of NH_3 and H_2S, which is important for complex purification of gas streams.

Special attention is paid to CO_2 capture on N-doped graphene. Depending on the configuration of nitrogen (graphite, pyridine, and pyrrole), the nature and energy of the interaction with the CO_2 molecule significantly changes. Pyrrole nitrogen exhibits the highest adsorption energy, which is associated with enhanced polarization of the CO_2 molecule and localization of electronic states in defective regions of the graphene lattice. Thus, Figure 8 clearly illustrates that the adsorption properties of graphene are determined not only by its high specific surface area, but also by the type of heteroatoms, defect configuration, and charge transfer mechanisms. CO_2 adsorption can occur by both physical and chemical mechanisms, depending on the nature of the adsorbent and the process conditions. On porous carbon materials, CO_2 adsorption occurs mainly through physical interactions, while micropores of 0.5–0.9 nm in size provide optimal capacity due to the effect of enhancing the adsorption potential. The adsorption capacity for CO_2 at atmospheric pressure and room temperature is usually 2–6 mmol/g for various carbon adsorbents. Chemical adsorption of CO_2 occurs on basic adsorbents, such as amino-containing materials, where carbamates and bicarbonates are formed [90,91]. Impregnation of adsorbents with metal catalysts, especially copper and palladium, significantly improves their ability to remove CO due to catalytic oxidation [92]. In this case, the process involves adsorption of CO on metal centers, followed by catalytic conversion to less toxic CO_2. This

approach makes it possible to achieve high CO removal efficiency (more than 90%) under relatively mild conditions.

4.2. Limitations and Prospects of Graphene Materials Application in Gas Adsorption

The adsorption properties of graphene significantly depend on the number of layers, the defect, and the nature of the surface modification. Monolayer graphene demonstrates maximum sensitivity and adsorption activity, whereas bi- and trilayer structures are characterized by a 30–50% decrease in capacity due to shielding of the active surface. The introduction of point defects forms local active centers with binding energy exceeding the values for the ideal basal plane by 50–200% with an optimal defect concentration of 0.1–1%. The edge regions of graphene have increased reactivity, while the armchair and zigzag configurations exceed the basal plane in terms of adsorption activity by 2–3 and 5–8 times, respectively.

Single Pt atoms coordinated with N-centers at a concentration of 0.1–2 wt.% provide selective adsorption of CO with an energy of 80–120 kJ/mol. Au nanoparticles 2–8 nm in size demonstrate selective adsorption of H_2S with an energy of 150–200 kJ/mol. The kinetics is limited by the surface reaction with rate constants: NO_2—0.8–2.5 min^{-1}, NH_3—0.3–1.2 min^{-1}, and SO_2—0.5–1.8 min^{-1}. The diffusion coefficients are H_2—10^{-4} cm^2/s, CO—10^{-6} cm^2/s, and NO_2—10^{-7} cm^2/s.

Maximum capacities at 298 K are NO_2—25–60 mg/g, NH_3—15–40 mg/g, SO_2—30–80 mg/g, H_2S—20–150 mg/g, and CO_2—50–120 mg/g. Selectivity coefficients are NO_2/N_2 = 80–250, SO_2/N_2 = 50–180, and NH_3/N_2 = 30–120. Resistive sensors show a resistance change of up to 200% for NO_2 with a detection limit of 0.5–5 ppb and a response time of less than 60 s. Field effect transistors show a current change of up to 300% at 100 ppb NO_2. Thermal regeneration is achieved at 150–600 °C, and photostimulated desorption by UV irradiation at 10–100 mW/cm^2 in 1–10 min. Cyclic stability exceeds 1000 cycles with a capacity loss of less than 15%. Liquid phase separation provides a productivity of 10–100 g/h at a cost of 10–50 USD·kg^{-1}.

Graphene was functionalized by plasma treatment in O_2, H_2, and Ar media, and the effects on the detection characteristics of NH_3 gas were evaluated [93]. O_2-plasma treatment induces graphene oxidation (graphoxide), while H_2-plasma causes hydrogenation (graphane). Graphane had the highest resistance of a sheet with a band gap of 3.0 eV. According to Melezhik A.V. et al. [94], graphene oxide demonstrates an adsorption capacity superior to carbon nanotubes due to its unique morphology, which ensures the accessibility of both sides of the graphene plane for the adsorption of pollutants, which contributes to the faster establishment of sorption equilibrium due to active elution of the adsorbent. The potential use of graphene oxide as a solid sorbent for the pre-concentration of trace elements and purification from heavy metal ions is due to its maximum adsorption capacity, which significantly exceeds the characteristics of existing sorbents. According to Ramezanzadeh M. et al. [95], the high adsorption characteristics of graphene oxide are associated with a large surface area and high capacity of oxygen-containing functional groups, the concentration of which can reach 30% by weight, which significantly exceeds the oxygen content in oxidized carbon nanotubes (usually no more than 5% by weight). Coordination bonds are formed between functional groups on the surface of graphene oxide and metal ions, ensuring effective adsorption.

However, Khiem et al. [96] emphasized that despite its high adsorption characteristics, graphene oxide has significant limitations associated with the implementation of the main part of adsorption interactions due to the electrostatic mechanism on the particle surface, which defines it as an adsorbent with a limited number of active sorption centers and limits its use in aqueous media with a high concentration of pollutants at a constant

amount sorbent. An additional disadvantage of graphene oxide is its hydrophilicity, which complicates separation and removal after the adsorption stage [97–99]. Obtaining an industrial commercial form of a multifunctional sorbent based on graphene oxide is difficult, since it demonstrates maximum sorption characteristics in the form of an aqueous suspension [100–102].

Considering the adsorption properties of graphene materials, it must be acknowledged that their practical application in gas purification faces serious challenges [103–105]. Despite the impressive theoretical characteristics, the adsorption energies of the main toxic gases (NO_2 18–25 kJ/mol, and NH_3 12–18 kJ/mol) turn out to be quite common for physisorption, and the lifetime of the adsorbed molecules of 10^{-9}–10^{-6} s requires constant stabilization of the process. The decrease in the capacity of multilayer graphene by 30–50% is particularly puzzling—it turns out that the most efficient monolayer material is at the same time the least technologically advanced for industrial production [106,107].

4.3. Comparative Analysis of Physico-Chemical, Sorption, and Economic Characteristics of Carbon Materials

The methodology for assessing the economic feasibility of carbon-based sorbents in this research is based on a mixed qualitative–quantitative approach, utilizing data from the literature sources and industry benchmarks. The analysis takes into account the key cost-forming factors relevant to various stakeholders involved in the production and application of gas sorbents, including the procurement of raw materials (such as biomass precursors, graphite, and catalysts), the energy consumption during the synthesis and activation processes (carbonization, chemical or physical activation, and CVD), and the expenses associated with surface modification and post-treatment. From the perspective of the end-user, the economic efficiency is determined by the adsorption capacity per unit mass, the adsorption kinetics, the regeneration efficiency, and the operational lifespan under cyclic conditions. Materials with moderate initial adsorption capacity but high regeneration stability and a long service life may therefore offer lower life cycle costs compared to materials with high capacity but limited durability. Additionally, environmental and sustainability considerations are taken into account, including the potential for regeneration, reuse, and environmentally responsible disposal of spent sorbents, as well as the use of renewable or waste-derived precursors.

The particle size of carbon sorbents is an important parameter that determines the kinetics of adsorption and the hydrodynamic characteristics of adsorption systems. Reducing the particle size reduces the diffusion path and accelerates mass transfer, while the range of 0.25–5 mm provides a compromise between effective kinetics and allowable hydraulic resistance in flow installations [108,109].

Surface modification significantly affects the sorption properties of carbon materials. Oxidative treatment increases the polarity of the surface by introducing oxygen-containing functional groups, whereas reductive heat treatment in an inert atmosphere increases hydrophobicity and promotes the adsorption of nonpolar compounds [110]. Alkaline activation at high temperatures leads to the development of microporosity and an increase in specific surface area to ~3000 m^2/g; however, the stability of such materials over long service cycles requires additional assessment.

The shape and morphology of carbon materials determine their kinetic characteristics. Fibrous activated carbons exhibit accelerated mass transfer due to a small diffusion pathway, and hierarchically porous structures provide an optimal combination of high capacity and improved pore accessibility. Composite systems based on carbon and zeolites or MOF are characterized by the synergistic effect of various adsorption mechanisms and increased selectivity.

Temperature has a dual effect on the adsorption process: an increase in temperature reduces the equilibrium capacity, but accelerates the kinetics. For most processes, the optimal range is 20–40 °C. The regeneration of carbon sorbents is effectively carried out by thermal, vapor, and microwave methods, ensuring the restoration of the adsorption capacity at the level of 90–95% in the initial cycles.

To systematize the differences between carbon materials, Table 2 presents their generalized physico-chemical characteristics. The analysis shows that activated carbons have the most balanced combination of specific surface area, stability, and cost, which explains their dominant position in industrial gas purification. Carbon nanotubes occupy an intermediate position in terms of sorption characteristics and cost, whereas graphene, despite its high theoretical potential, is limited by technological and economic factors. Fullerenes are characterized by a minimal specific surface area and are of limited importance for adsorption applications. Pore characteristics reveal distinct patterns among carbon-based materials. Carbon nanotubes exhibit the highest pore volume (0.5–2.0 cm^3/g) due to their hollow cylindrical structure, which facilitates efficient mass transfer. Composite materials show the widest range (0.4–2.5 cm^3/g), reflecting the ability to tailor their structure. Graphene is virtually non-porous, and its adsorption properties are governed primarily by surface interactions. Activated carbon displays typical pore volumes of 0.3–1.5 cm^3/g, characteristic of micro- and mesoporous materials.

Table 2. General physico-chemical characteristics of carbon materials.

Property	Activated Carbon	Carbon Nanotubes	Graphene	Fullerene	Composite Materials	Refs.
Specific surface area (m^2/g)	500–1500	200–900	500–2630	40–80	300–2000	[3,23]
Pore volume (cm^3/g)	0.3–1.5	0.5–2.0	0–0.8	0.1–0.5	0.4–2.5	[30,39]
Pore size (nm)	0.5–50	1–50	Absent	Molecular	Hierarchical	[44,46,76]
Density (g/cm^3)	0.4–0.9	0.8–1.8	2.2	1.7	0.5–2.0	[78,84,106]

Economic analysis shows a clear correlation between the complexity of production and the cost of materials. Activated carbon remains the most affordable at a price of 2–15 USD·kg^{-1} due to proven technologies and affordable raw materials. Composite materials occupy a niche of 20–200 USD·kg^{-1}, offering improved performance with a moderate increase in cost. Nanotubes and graphene are in the range of 50–500 USD·kg^{-1} and 100–1000 USD·kg^{-1}, respectively, reflecting the complexity of their synthesis and the relative novelty of the technology. Fullerenes remain the most expensive at 500–5000 USD·kg^{-1} due to specialized production and limited demand.

The ratio of efficiency and cost reveals different niches of materials application. Composite materials demonstrate an optimal balance of characteristics, allowing for a significant improvement in properties at an acceptable cost increase. Activated carbon retains its dominant position in mass applications due to its proven efficiency and low cost. Graphene and nanotubes justify their high cost only in high-tech solutions where maximum performance is critical. It is advisable to use fullerenes only in highly specialized tasks, where their unique properties cannot be replaced by cheaper alternatives. Let us present a comparison of carbon materials in terms of cost in Table 3:

Activated carbon occupies a leading position in terms of economic efficiency with a price of 2–15 USD·kg^{-1} due to proven production technologies and affordable raw materials. Centuries of experience in use and ease of scaling ensure consistently low costs, which explains the material's dominance in industrial applications for processing large volumes of gases. Composite materials in the range of 20–200 USD·kg^{-1} offer an optimal price-performance ratio. The ability to customize properties for specific tasks justifies a

3–10-fold increase in cost compared to activated carbon. The moderate modification costs of 5–50 USD·kg^{-1} make composites attractive for long-term projects.

Table 3. Cost indicators of carbon materials.

Cost Indicator	Activated Carbon	Carbon Nanotubes	Graphene	Fullerene	Composite Materials	Refs.
Material cost (USD·kg^{-1})	2–15	50–500	100–1000	500–5000	20–200	[6,12,19,22,29]
Modification cost (USD·kg^{-1})	1–10	10–100	50–300	100–1000	5–50	[40,46,58,72,88,98]

Nanotubes (50–500 USD·kg^{-1}) and graphene (100–1000 USD·kg^{-1}) are in a high price category due to the complexity of synthesis and small production volumes. Multi-walled nanotubes are cheaper than single-walled ones, and graphene oxide is much more affordable than CVD graphene. High modification costs (10–300 USD·kg^{-1}) further increase the total cost of the system. Fullerenes represent a premium segment with prices of 500–5000 USD·kg^{-1}. C_{60} is relatively affordable, while functionalized fullerenes reach maximum prices. The economic justification of the application is possible only in highly specialized high-tech areas. A life cycle cost analysis shows that at high concentrations of pollutants, activated carbon provides a minimum cost of 0.5–2.0 USD·kg^{-1} of treated gas. At low concentrations, the advantage shifts to more expensive materials due to their high selectivity. Composites demonstrate stable efficiency over the entire range of conditions, which explains their growing market share.

Based on the data presented in Table 4, it should be noted that the carbon materials market is clearly divided between traditional and innovative applications. Activated carbon dominates classical cleaning technologies at 70% of the air purification market, 65% of water purification, and 55% of automotive applications, due to its low cost and proven effectiveness. Petrochemicals and military technologies remain practically a monopoly of activated carbon due to proven standards and safety requirements.

Table 4. Main applications of carbon materials.

Industry	AC	CNTs	Graphene	Fullerene	Composites	Market Leader	Refs.
Air purification	Dominant	Active	Weak	Not used	Widely applied	AC (70% of market)	[5,6]
Water treatment	Dominant	Active	Active	Weak	Widely applied	AC (65% of market)	[18,22]
Energy	Active	Dominant	Dominant	Weak	Widely applied	Graphene/CNTs	[33,46]
Automotive	Dominant	Widely applied	Weak	Not used	Widely applied	AC (55% of market)	[57,75]
Electronics	Weak	Dominant	Dominant	Weak	Active	Graphene/CNTs	[88,91]
Petrochemicals	Dominant	Active	Weak	Not used	Widely applied	AC (dominant)	[96,101]
Medicine	Widely applied	Active	Active	Active	Active	AC (detoxification)	[109,110]
Military technologies	Dominant	Active	Active	Weak	Widely applied	AC (PPE)	[111,112]

Carbon nanotubes and graphene are taking over high-tech industries such as energy and electronics, where their superior electrical properties are critically important. These materials are growing at a rate of 15–40% per year versus 3–5% for activated carbon, which indicates a shift in technological priorities. Composite materials demonstrate versatility, being actively used in all industries with a growth of 20–30% per year, which makes them a transitional link between traditional and revolutionary solutions.

Fullerenes are limited to applications in medicine and specialized electronics due to their high cost, but they show stable growth of 5–10% per year. Medicine remains the only industry with an even distribution of all types of carbon materials, reflecting the diversity of medical tasks and the willingness of the field to innovate.

Table 5 shows the main barriers to the introduction of carbon materials.

Table 5. Main barriers to the implementation of carbon materials.

Material	Main Barriers	Solutions	Refs.
AC CNTs Graphene	Limited selectivity High cost Technological challenges	Surface modification Production scaling New synthesis methods	[35,46] [49,57,75] [78,89]
Fullerenes	Very high cost Processing complexity	Niche applications Design for recycling	[100,103] [105,112]
Material	**Main Barriers**	**Solutions**	**Refs.**
AC CNTs Graphene	Limited selectivity High cost Technological challenges	Surface modification Production scaling New synthesis methods	[35,46] [49,57,75] [78,89]
Fullerenes	Very high cost Processing complexity	Niche applications Design for recycling	[100,103] [105,112]

Activated carbon is limited by non-selectivity—it adsorbs all substances indiscriminately, without distinguishing between desired and undesired components. This can be addressed through chemical surface modification to create selective adsorption sites. Carbon nanotubes and graphene are costly due to complex production processes at extreme temperatures and low product yields; the price of nanotubes is 50–100 times higher than that of activated carbon. This barrier can be mitigated by scaling up production and improving synthesis technologies. Graphene additionally suffers from quality issues, as commercial material contains numerous defects that reduce its unique properties. Most "graphene" available on the market is defective and exhibits limited performance. Fullerenes remain an exotic material because of extremely expensive production with low yield, restricting their use to niche applications where the high cost is justified by special properties. Composites face recycling challenges, as their components are strongly bonded, making reuse nearly impossible and raising environmental concerns at the end of their life cycle.

The carbon nanomaterials market will reach $5.7 billion by 2030 with growth of 17.2% per year [111–113], concentrating in the energy sector with a volume of 662 USD million and growth of 23.9% per year. These projections provide an economic rationale for the large-scale development of advanced sorption technologies, which is consistent with recent peer-reviewed analyses emphasizing cost reduction trends and scalability challenges of carbon nanomaterials [5,31].

Nanotube–graphene hybrids demonstrate synergistic effects in sensors and actuators [105,106], creating self-adapting filtration systems [114]. Nanoresonators reach terahertz frequencies with the detection of individual molecules [115–117], turning adsorption into an intelligent feedback process.

Machine learning reduces the development time of composites from months to weeks by predicting properties before synthesis. Digital twins optimize processes without physical experiments, which is critical for expensive nanomaterials. Additive manufacturing creates personalized filters with controlled pore geometry for specific operating conditions.

Direct CO_2 capture requires an increase in current capacity from 0.0385 to 20 Gt of CO_2 per year [118,119]. This stimulates the development of materials with extreme selectivity to low concentrations, where composites with programmable porosity show maximum potential. Smart textile materials integrate monitoring and protection from toxic gases into clothing [120–122], creating a market for personalized protection for workers in hazardous industries and residents of polluted megacities. Graphene composites displace nanotubes due to their ease of handling [123–127].

Graphene's 70% reduction in cost by 2030 makes it competitive with activated carbon in high-tech applications. Self-healing materials with catalytic nanoparticles will ensure continuous regeneration without external heating. Biomimetic structures can reach the theoretical limits of adsorption efficiency by copying natural filtration mechanisms.

Scaling is hindered by the production of high-quality graphene without loss of properties and the lack of standardization for mission-critical industries. The future will be determined by the creation of integrated systems that combine adsorption, catalytic decomposition, and intelligent control into an autonomous cycle.

The particle size and shape of carbon materials critically affect their sorption properties through kinetic effects, equilibrium capacity, and hydrodynamic characteristics. Reducing the particle size from 5 mm to 0.1 mm reduces the diffusion path by 50 times and the time to reach equilibrium from several hours to 10–30 min, while the optimal size for industrial applications is 0.25–5 mm as a compromise between mass transfer efficiency and hydraulic resistance.

Metallic activation by transition metals (Cu, Ni, Ag, Pd, and Pt) provides catalytic oxidation of toxic gases, dissociative adsorption, and formation of intermetallic compounds [128]. Copper is effective for the oxidation of CO and the adsorption of H_2S through the formation of CuS [129], nickel catalyzes the hydrogenation and dissociative adsorption of H_2 [130], silver provides antimicrobial properties and oxidation of olefins, and palladium and platinum demonstrate the highest catalytic activity in oxidative reactions [131,132].

Nonmetallic activation includes nitrogen activation with ammonia at 800–900 °C to introduce pyridine, pyrrole, and graphite nitrogen, which increases surface elasticity and selective co_2 adsorption by up to 150%. Phosphoric activation of H_3PO_4 develops mesoporosity and improves the adsorption of large organic molecules, sulfur activation provides selectivity to thiocompounds and improves mercury adsorption, and boric activation introduces electron acceptor centers for selective adsorption of NH_3 and amines.

Combined activation of metal–nonmetal systems (Ni-N, Cu-S) provides a synergistic effect and bifunctional activity, while optimizing temperature conditions (300–500 °C to preserve functional groups, 800–1000 °C to form stable bonds) and control of the activation medium (inert, reducing, and oxidizing) make it possible to purposefully modify the properties of carbon compounds and sorbents for specific applications.

5. Conclusions

Carbon materials exhibit excellent adsorption characteristics for a wide range of toxic gases due to their high specific surface area (up to 3000 m^2/g for activated carbons, 1315 m^2/g for single-layer carbon nanotubes, 2630 m^2/g for graphene) and advanced porous structure, while composite systems provide a synergistic effect exceeding the characteristics of individual components by 20–50%.

Physical adsorption through van der Waals interactions dominates for most organic vapors with energies of 20–60 kJ/mol, chemical adsorption (40–200 kJ/mol) provides high selectivity with difficulty in regeneration, and capillary condensation in mesopores is significant at high relative pressures. Micropores determine the main adsorption capacity for small molecules, and mesopores provide transport and accessibility of the inner surface, while the optimal particle size is 0.25–5 mm for industrial applications.

Covalent functionalization (oxidation, amidation, and esterification) makes it possible to purposefully change surface properties, doping with heteroatoms radically changes the electronic structure and selectivity, and metallic activation provides catalytic properties and improves regeneration. Nitrogen-doped CNTs (up to 4.5 mmol) are most effective for CO_2/g) and CNT-MOF composites (8–15 mmol/g); for NH_3, high selectivity is achieved on

acid-modified materials; for NO_x, functionalization by amino groups provides selectivity to NO_2; and for H_2S, adsorption on metal-modified carbons is effective.

The cost of materials ranges from 2 to 5 USD·kg^{-1} for activated carbon to 50–200 USD·kg^{-1} for CNT composites and 100–500 USD·kg^{-1} for graphene composites, while economic efficiency is achieved due to increased selectivity, capacity, and extended service life with a projected reduction in the cost of nanotubes and graphene by 50–70% by 2030. The kinetics of adsorption is described by first/second order models with an equilibrium time from minutes to hours, thermal regeneration at 100–200 °C provides 90–95% efficiency, and microwave and vapor regeneration show prospects for energy conservation.

Promising areas include the creation of hierarchically porous structures to optimize mass transfer, the development of self-healing materials to increase service life, the creation of multifunctional systems for simultaneous capture, transformation, and detection, and integration with machine learning for rational material design. DFT calculations are effective for determining interaction energies and adsorption mechanisms, GCMC modeling adequately predicts adsorption capacities, and combining experimental and theoretical approaches accelerates the development of new materials.

Practical applications include industrial gas purification with high efficiency at high volumes, automotive filters with compactness and selectivity, personal protective equipment with lightness and high protective ability, and gas sensors with fast response and high sensitivity up to 10 ppb, which confirms the versatility and promise of carbon materials for solving problems of gas purification and detection of toxic substances.

Future research on carbon-based adsorbents is expected to focus on the optimization of adsorption kinetics and dynamic mechanisms under realistic conditions. The development of hierarchically porous structures and multifunctional composites will enhance mass transfer, selectivity, and regeneration efficiency. Advanced modeling approaches, such as DFT calculations and GCMC simulations, combined with experimental studies, will allow accurate prediction of adsorption energies, capacities, and competitive interactions in multicomponent gas streams. Integration of machine learning and data-driven design strategies promises to accelerate the discovery of next-generation carbon materials, while kinetic studies will provide essential guidance for scaling laboratory results to industrial applications. Emphasis on energy-efficient regeneration methods and long-term stability will be key to translating these materials into sustainable, high-performance gas capture and sensing technologies.

Author Contributions: Conceptualization N.A. and M.A.; methodology A.S., L.F.V. and Y.D.; validation A.K., G.I., A.S., Y.Y.; formal analysis N.A.; investigation N.A. and A.K.; writing—original draft preparation M.A.; writing—review and editing A.S. and M.A. visualization L.F.V. and Y.D., Y.Y.; supervision A.K.; project administration Y.D., L.F.V. and M.A. All authors have read and agreed to the published version of the manuscript.

Funding: This work was supported by the Ministry of Science and Higher Education of the Republic of Kazakhstan grant (AP22786556).

Institutional Review Board Statement: Not applicable.

Informed Consent Statement: Not applicable.

Data Availability Statement: Not applicable.

Conflicts of Interest: The authors declare no conflicts of interest.

Abbreviations

The following abbreviations are used in this manuscript:

CNTs	Carbon nanotubes
MWCNTs	Multi-walled carbon nanotubes
GCMC	Grand Canonical Monte Carlo
DFT	Density Functional Theory

References

1. Filonchyk, M.; Peterson, M.P.; Zhang, L.; Hurynovich, V.; He, Y. Greenhouse gases emissions and global climate change: Examining the influence of CO_2, CH_4, and N_2O. *Sci. Total Environ.* **2024**, *935*, 173359. [CrossRef]
2. Zhang, Y.; Yang, X.; Han, J.; Tian, J.; Zhang, T.; Li, Y.; Zhang, J.; Shi, Y.; Zhang, J. Screening of Pure ILs and DESs for CO_2 Separation, N_2O Separation, and H_2S Separation Processes. *Int. J. Chem. Eng.* **2023**, *2023*, 8691957. [CrossRef]
3. Kustov, A.L.; Kustov, L.M. IR-spectroscopic study of complex formation of nitrogen oxides (NO, N_2O) with cationic forms of zeolites and the reactivity of adsorbed species in CO and CH_4 oxidation. *Molecules* **2021**, *27*, 55. [CrossRef]
4. Bannov, A.G.; Trubin, I.V.; Zakharov, I.K.; Maksimovskiy, E.A.; Kurmashov, P.B. A critical review on soil gas analysis: Modern technologies and problems. *Agronomy* **2024**, *14*, 2374. [CrossRef]
5. Reddy, M.S.B.; Ponnamma, D.; Sadasivuni, K.K.; Kumar, B.; Abdullah, A.M. Carbon dioxide adsorption based on porous materials. *RSC Adv.* **2021**, *11*, 12658–12681. [CrossRef]
6. Ajmal, Z.; Ali, H.; Ullah, S.; Kumar, A.; Abboud, M.; Gul, H.; Al-hadeethi, Y.; Alshammari, A.S.; Almuqati, N.; Ashraf, G.A.; et al. Use of carbon-based advanced materials for energy conversion and storage applications: Recent development and future outlook. *Fuel* **2024**, *367*, 131295. [CrossRef]
7. Li, Q.; Zhang, H.; Peng, F.; Wang, C.; Li, H.; Xiong, L.; Guo, H.; Chen, X. Monoethanolamine-modified attapulgite-based amorphous silica for the selective adsorption of CO_2 from simulated biogas. *Energy Fuels* **2020**, *34*, 2097–2106. [CrossRef]
8. Ghaemi, A.; Mashhadimoslem, H.; Zohourian Izadpanah, P. NiO and MgO/activated carbon as an efficient CO_2 adsorbent: Characterization, modeling, and optimization. *Int. J. Environ. Sci. Technol.* **2022**, *19*, 727–746. [CrossRef]
9. Cucu, E.; Dalkılıç, E.; Altundas, R.; Sadak, A.E. Gas sorption and selectivity study of N, N, N′, N′-tetraphenyl-1, 4-phenylenediamine based microporous hyper-crosslinked polymers. *Microporous Mesoporous Mater.* **2022**, *330*, 111567. [CrossRef]
10. Chataut, G.; Bhatta, B.; Joshi, D.; Subedi, K.; Kafle, K. Greenhouse gases emission from agricultural soil: A review. *J. Agric. Food Res.* **2023**, *11*, 100533. [CrossRef]
11. Nielsen, K.S.; Nicholas, K.A.; Creutzig, F.; Dietz, T.; Stern, P.C. The role of high-socioeconomic-status people in locking in or rapidly reducing energy-driven greenhouse gas emissions. *Nat. Energy* **2021**, *6*, 1011–1016. [CrossRef]
12. Romero, J.P.; Gramkow, C. Economic complexity and greenhouse gas emissions. *World Dev.* **2021**, *139*, 105317. [CrossRef]
13. Lamb, W.F.; Grubb, M.; Diluiso, F.; Minx, J.C. Countries with sustained greenhouse gas emissions reductions: An analysis of trends and progress by sector. *Clim. Policy* **2022**, *22*, 1–17. [CrossRef]
14. Brissaud, C.; Jain, S.; Henrotte, O.; Pouget, E.; Pauly, M.; Naldoni, A.; Comesaña-Hermo, M. Plasmonic Chirality Meets Reactivity: Challenges and Opportunities. *J. Phys. Chem. C* **2025**, *129*, 3361–3373. [CrossRef]
15. Sadraei, R.; Cucchiara, F.; Magnacca, G.; Testa, M.L. Surface functionalization of handleable silica-based mesoporous materials for CO_2 sequestration: Synthesis, characterization and performance. *Surf. Interfaces* **2021**, *27*, 101542. [CrossRef]
16. Ramirez-de-Arellano, J.M.; Canales, M.; Magaña, L.F. Carbon nanostructures doped with transition metals for pollutant gas adsorption systems. *Molecules* **2021**, *26*, 5346. [CrossRef] [PubMed]
17. Deji, R.; Verma, A.; Kaur, N.; Choudhary, B.C.; Sharma, R.K. Density functional theory study of carbon monoxide adsorption on transition metal doped armchair graphene nanoribbon. *Mater. Today Proc.* **2022**, *54*, 771–776. [CrossRef]
18. Alemi, F.M.; Mohammadi, S.; Dehghani, S.A.M.; Rashidi, A.; Hosseinpour, N.; Seif, A. Experimental and DFT studies on the effect of carbon nanoparticles on asphaltene precipitation and aggregation phenomena. *Chem. Eng. J.* **2021**, *422*, 130030. [CrossRef]
19. Mollaamin, F.; Monajjemi, M. Doping of graphene nanostructure with iron, nickel and zinc as selective detector for the toxic gas removal: A density functional theory study. *C* **2023**, *9*, 20. [CrossRef]
20. Torrent, M. Density-Functional Theory Electronic Structure Calculations Within the "Projector Augmented-Wave" Approach. Ph.D. Thesis, Université Paris-Saclay, Gif-sur-Yvette, France, 2024.
21. Makkar, P.; Ghosh, N.N. A review on the use of DFT for the prediction of the properties of nanomaterials. *RSC Adv.* **2021**, *11*, 27897–27924. [CrossRef]
22. Idrissi, S.; Labrim, H.; Bahmad, L.; Benyoussef, A. DFT and TDDFT studies of the new inorganic perovskite $CsPbI_3$ for solar cell applications. *Chem. Phys. Lett.* **2021**, *766*, 138347. [CrossRef]
23. Pawar, P.; Anumalla, S.; Sharma, S. Role of carbon nanotubes (CNTs) in transgenic plant development. *Biotechnol. Bioeng.* **2023**, *120*, 3493–3500. [CrossRef]

24. Zaumseil, J. Luminescent Defects in Single-Walled Carbon Nanotubes for Applications. *Adv. Opt. Mater.* **2022**, *10*, 2101576. [CrossRef]
25. Gellman, A.J. An account of chiral metal surfaces and their enantiospecific chemistry. *Acc. Mater. Res.* **2021**, *2*, 1024–1032. [CrossRef]
26. Xiang, Y.; Zhang, L.; Liu, C. Electrical properties of carbon nanotubes: From individual to assemblies. *Nanomaterials* **2025**, *15*, 1165. [CrossRef]
27. Somu, C.; Karthi, A.; Singh, S.; Karthikeyan, R.; Dinesh, S.; Ganesh, N. Synthesis of various forms of carbon nanotubes by arc discharge methods—Comprehensive review. *Int. Res. J. Eng. Technol.* **2017**, *4*, 344–354.
28. Sivakumar, V.M.; Mohamed, A.R.; Abdullah, A.Z.; Chai, S.P. Role of reaction and factors of carbon nanotubes growth in chemical vapour decomposition process using methane—A highlight. *J. Nanomater.* **2010**, *2010*, 395191. [CrossRef]
29. Azari, A.; Nabizadeh, R.; Nasseri, S.; Mahvi, A.H.; Mesdaghinia, A.R. Comprehensive systematic review and meta-analysis of dyes adsorption by carbon-based adsorbent materials: Classification and analysis of last decade studies. *Chemosphere* **2020**, *250*, 126238. [CrossRef] [PubMed]
30. Ding, X.; Yang, S.; Zhou, S.; Zhan, Y.; Lai, Y.; Zhou, X.; Xu, X.; Nie, H.; Huang, S.; Yang, Z. Biomimetic molecule catalysts to promote the conversion of polysulfides for advanced lithium–sulfur batteries. *Adv. Funct. Mater.* **2020**, *30*, 2003354. [CrossRef]
31. Gusain, R.; Kumar, N.; Ray, S.S. Recent advances in carbon nanomaterial-based adsorbents for water purification. *Coord. Chem. Rev.* **2020**, *405*, 213111. [CrossRef]
32. Khoshraftar, Z.; Ghaemi, A.; Hemmati, A. Comprehensive investigation of isotherm, RSM, and ANN modeling of CO_2 capture by multi-walled carbon nanotube. *Sci. Rep.* **2024**, *14*, 5130. [CrossRef]
33. Kohmuean, P.; Inthomya, W.; Wongkoblap, A.; Tangsathitkulchai, C. Monte Carlo simulation experimental studies of, CO_2, CH_4; their mixture capture in porous carbons. *Molecules* **2021**, *26*, 2413. [CrossRef] [PubMed]
34. Kuznetsova, T.S.; Burakov, A.E.; Pasko, T.V.; Burakova, I.V.; Dyachkova, T.P.; Memetova, A.E. Physicochemical and sorption properties of nanocomposite aerogel based on modified carbon nanotubes and graphene. *Chem. Chem. Technol.* **2023**, *66*, 66–76.
35. Liu, Y.; Jiang, J.; Pu, Y.; Francisco, J.S.; Zeng, X.C. Evidence of formation of 1–10 nm diameter ice nanotubes in double-walled carbon nanotube capillaries. *ACS Nano* **2023**, *17*, 6922–6931. [CrossRef]
36. Kocaman, S. Evaluation of adsorption characteristics of new-generation CNT-based adsorbents: Characterization, modeling, mechanism, and equilibrium study. *Carbon Lett.* **2023**, *33*, 883–897. [CrossRef]
37. Saxena, M.; Sharma, N.; Saxena, R. Highly efficient and rapid removal of a toxic dye: Adsorption kinetics, isotherm, and mechanism studies on functionalized multiwalled carbon nanotubes. *Surf. Interfaces* **2020**, *21*, 100639. [CrossRef]
38. Ali, I.; Alharbi, O.M.; ALOthman, Z.A.; Al-Mohaimeed, A.M.; Alwarthan, A. Modeling of fenuron pesticide adsorption on CNTs for mechanistic insight and removal in water. *Environ. Res.* **2019**, *170*, 389–397. [CrossRef]
39. Bassyouni, M.; Mansi, A.E.; Elgabry, A.; Ibrahim, B.A.; Kassem, O.A.; Alhebeshy, R. Utilization of carbon nanotubes in removal of heavy metals from wastewater: A review of the CNTs' potential and current challenges. *Appl. Phys. A* **2020**, *126*, 38. [CrossRef]
40. Pan, B.O.; Xing, B. Adsorption mechanisms of organic chemicals on carbon nanotubes. *Environ. Sci. Technol.* **2008**, *42*, 9005–9013. [CrossRef]
41. Bahmanzadgan, F.; Ghaemi, A.; Qasemnazhand, M.; Molaee, M. Simulation of gas adsorption on single-walled carbon nanotubes. *Sci. Rep.* **2025**, *15*, 15595. [CrossRef]
42. Nasr, G.E.; Baiomy, M.A.; Taieb, A.Z.; Abdel Razek, M.E.; Refai, M. Assessment of the performance of Ni carbon nanotube nano composite coatings and activated carbon for diesel exhaust treatment. *Sci. Rep.* **2025**, *15*, 4477. [CrossRef]
43. Xu, Y.; Rosa, A.; Liu, X.; Su, D. Characterization and use of functionalized carbon nanotubes for the adsorption of heavy metal anions. *New Carbon Mater.* **2011**, *26*, 57–62. [CrossRef]
44. Yan, T.; Li, T.X.; Wang, R.Z.; Jia, R. Experimental investigation on the ammonia adsorption and heat transfer characteristics of the packed multi-walled carbon nanotubes. *Appl. Therm. Eng.* **2015**, *77*, 20–29. [CrossRef]
45. Martínez-Ahumada, E.; Díaz-Ramírez, M.L.; Velásquez-Hernández, M.D.J.; Jancik, V.; Ibarra, I.A. Capture of toxic gases in MOFs: SO_2, H_2S, NH_3 and NO_x. *Chem. Sci.* **2021**, *12*, 6772–6799. [CrossRef] [PubMed]
46. Zeng, G.; Guo, S.; Zhai, X. Experimental study on adsorption of SO_2 and NH_3 by activated carbon with monometallic active sites at low concentration under room temperature. *ACS Omega* **2024**, *9*, 5523–5533. [CrossRef] [PubMed]
47. Cherevotan, A.; Raj, J.; Peter, S.C. An overview of porous silica immobilized amines for direct air CO_2 capture. *J. Mater. Chem. A* **2021**, *9*, 27271–27303. [CrossRef]
48. Fan, L.-Q.; Tu, Q.-M.; Geng, C.-L.; Wang, Y.-L.; Sun, S.-J.; Huang, Y.-F.; Wu, J.-H. Improved redox-active ionic liquid-based ionogel electrolyte by introducing carbon nanotubes for application in all-solid-state supercapacitors. *Int. J. Hydrogen Energy* **2020**, *45*, 17131–17139. [CrossRef]
49. Popova, A.A.; Shubin, I.N. Technology for modifying sorbents based on zeolite with carbon nanotubes. *Vestn. Tambov. Gos. Teh. Univ.* **2021**, *27*, 661. [CrossRef]

50. Buzaeva, M.V.; Makarova, I.A.; Vaganova, E.S.; Davydova, O.A.; Sud'in, Y.I.; Sergeev, V.A. Surface modification of multiwalled carbon nanotubes to impart technological properties. *Rev. Adv. Chem.* **2023**, *13*, 160–166. [CrossRef]
51. Harimech, Z.; Hairch, Y.; Atamanov, M.; Toshtay, K.; Azat, S.; Souhair, N.; Amrousse, R. Carbon Nanotube Iridium-Cupric Oxide Supported Catalysts for Decomposition of Ammonium Dinitramide in the Liquid Phase. *Int. J. Energetic Mater. Chem. Propuls.* **2023**, *22*, 13–18. [CrossRef]
52. Mansurov, Z.A.; Atamanov, M.K.; Elemesova, Z.; Lesbaev, B.T.; Chikradze, M.N. New Nanocarbon High-Energy Materials. *Combust. Explos. Shock. Waves* **2019**, *55*, 402–408. [CrossRef]
53. Mansurov, Z.A.; Lodewyckx, P.; Velasco, L.F.; Azat, S.; Kerimkulova, A.R. Modified sorbents based on walnet shell for sorption of toxic gases. *Mater. Today Proc.* **2021**, *49*, 2521–2526. [CrossRef]
54. Atamanov, M.K.; Amrousse, R.; Jandosov, J.; Hori, K.; Kerimkulova, A.R.; Chenchik, D.I.; Kolesnikov, B.Y. Combustion Characteristics of HAN-Based Green Propellant Assisted with Nanoporous Active Carbons. *Eurasian Chem. Technol. J.* **2017**, *19*, 215–222. [CrossRef]
55. Pui, W.K.; Yusoff, R.; Aroua, M.K. A review on activated carbon adsorption for volatile organic compounds (VOCs). *Rev. Chem. Eng.* **2018**, *35*, 649–668. [CrossRef]
56. Sultana, M.; Rownok, M.H.; Sabrin, M.; Rahaman, M.H.; Alam, S.N. A review on experimental chemically modified activated carbon to enhance dye and heavy metals adsorption. *Clean. Eng. Technol.* **2022**, *6*, 100382. [CrossRef]
57. Wawrzyńczak, D.; Panowski, M.; Majchrzak-Kucęba, I. Possibilities of CO_2 purification coming from oxy-combustion for enhanced oil recovery and storage purposes by adsorption method on activated carbon. *Energy* **2019**, *180*, 787–796. [CrossRef]
58. Jiang, L.; Gonzalez-Diaz, A.; Ling-Chin, J.; Roskilly, A.P.; Smallbone, A.J. Post-combustion CO_2 capture from a natural gas combined cycle power plant using activated carbon adsorption. *Appl. Energy* **2019**, *245*, 1–15. [CrossRef]
59. Jedli, H.; Almonnef, M.; Rabhi, R.; Mbarek, M.; Abdessalem, J.; Slimi, K. Activated carbon as an adsorbent for CO_2 capture: Adsorption, kinetics, and RSM modeling. *ACS Omega* **2023**, *9*, 2080–2087. [CrossRef]
60. Taurbekov, A.; Abdisattar, A.; Atamanov, M.; Yeleuov, M.; Daulbayev, C.; Askaruly, B.K.; Mansurov, Z.; Castro-Gutierrez, J.; Celzard, A.; Fierro, V.; et al. Biomass-Derived Highly Porous Carbon via CO_2 Activation for Supercapacitor Electrodes. *J. Compos. Sci.* **2023**, *7*, 444. [CrossRef]
61. Chun, S.-E.; Whitacre, J.F. Formation of micro/mesopores during chemical activation in tailor-made nongraphitic carbons. *Microporous Mesoporous Mater.* **2017**, *251*, 34–41. [CrossRef]
62. Patel, H.; Weldekidan, H.; Mohanty, A.; Misra, M. Effect of physicochemical activation on CO_2 adsorption of activated porous carbon derived from pine sawdust. *Carbon Capture Sci. Technol.* **2023**, *8*, 100128. [CrossRef]
63. Shahcheragh, S.K.; Bagheri Mohagheghi, M.M.; Shirpay, A. Effect of physical and chemical activation methods on the structure, optical absorbance, band gap and urbach energy of porous activated carbon. *SN Appl. Sci.* **2023**, *5*, 313. [CrossRef]
64. Azat, S.; Busquets, R.; Pavlenko, V.V.; Kerimkulova, A.R.; Whitby, R.L.; Mansurov, Z.A. Applications of activated carbon sorbents based on greek walnut. *Appl. Mech. Mater.* **2014**, *467*, 49–51.
65. Giraldo, L.; Vargas, D.P.; Moreno-Piraján, J.C. Study of CO_2 adsorption on chemically modified activated carbon with nitric acid and ammonium aqueous. *Front. Chem.* **2020**, *8*, 543452. [CrossRef]
66. Vega, M.F.; Diaz-Faes, E.; Barriocanal, C. Kinetic and Mechanistic Study of CO_2 Adsorption on Activated Hydrochars. *J. CO_2 Util.* **2024**, *81*, 102716. [CrossRef]
67. Lodewyckx, P.; Raymundo-Piñero, E.; Vaclavikova, M.; Berezovska, I.; Thommes, M.; Béguin, F.; Dobos, G. Suggested improvements in the parameters used for describing the low relative pressure region of the water vapour isotherms of activated carbons. *Carbon* **2013**, *60*, 556–558. [CrossRef]
68. Velasco, L.F.; Snoeck, D.; Mignon, A.; Misseeuw, L.; Ania, C.O.; Van Vlierberghe, S.; Dubruel, P.; de Belie, N.; Lodewyckx, P. Role of the surface chemistry 216 of the adsorbent on the initialization step of the water sorption process. *Carbon* **2016**, *106*, 284–288. [CrossRef]
69. Gebreegziabher, T.B.; Wang, S.; Nam, H. Adsorption of H_2S, NH_3 and TMA from indoor air using porous corncob activated carbon: Isotherm and kinetics study. *J. Environ. Chem. Eng.* **2019**, *7*, 103234. [CrossRef]
70. Castrillon, M.C.; Moura, K.O.; Alves, C.A.; Bastos-Neto, M.; Azevedo, D.C.S.; Hofmann, J.; Möllmer, J.; Einicke, W.-D.; Gläser, R. CO_2 and H_2S removal from CH_4-rich streams by adsorption on activated carbons modified with K_2CO_3, NaOH, or Fe_2O_3. *Energy Fuels* **2016**, *30*, 9596–9604. [CrossRef]
71. Safri, A.; Fletcher, A.J.; Safri, R.; Rasheed, H. Integrated adsorption–photodegradation of organic pollutants by carbon xerogel/titania composites. *Molecules* **2022**, *27*, 8483. [CrossRef]
72. Xu, Y.; Chen, Y.; Ma, C.; Qiao, W.; Wang, J.; Ling, L. Functionalization of activated carbon fiber mat with bimetallic active sites for NH_3 and H_2S adsorption at room temperature. *Sep. Purif. Technol.* **2022**, *303*, 122335. [CrossRef]
73. Wang, S.; Xu, S.; Gao, S.; Xiao, P.; Jiang, M.; Zhao, H.; Huang, B.; Liu, L.; Niu, H.; Wang, J.; et al. Simultaneous removal of SO_2 and NO_x from flue gas by low-temperature adsorption over activated carbon. *Sci. Rep.* **2021**, *11*, 11003. [CrossRef]

74. Lodewyckx, P.; Wood, G.O.; Ryu, S.K. The Wheeler–Jonas equation: A versatile tool for the prediction of carbon bed breakthrough times. *Carbon* **2004**, *42*, 1351–1355. [CrossRef]
75. Ramalingam, G.; Priya, A.K.; Gnanasekaran, L.; Rajendran, S.; Hoang, T.K. Biomass and waste derived silica, activated carbon and ammonia-based materials for energy-related applications—A review. *Fuel* **2024**, *355*, 129490. [CrossRef]
76. Phothong, K.; Tangsathitkulchai, C.; Lawtae, P. The analysis of pore development and formation of surface functional groups in bamboo-based activated carbon during CO_2 activation. *Molecules* **2021**, *26*, 5641. [CrossRef]
77. Ghouma, I.; Jeguirim, M.; Limousy, L.; Bader, N.; Ouederni, A.; Bennici, S. Factors influencing NO_2 adsorption/reduction on microporous activated carbon: Porosity vs. surface chemistry. *Materials* **2018**, *11*, 622. [CrossRef] [PubMed]
78. Niu, Y.; Zheng, C.; Xie, Y.; Kang, K.; Song, H.; Bai, S.; Han, H.; Li, S. Efficient adsorption of ammonia by surface-modified activated carbon fiber mesh. *Nanomaterials* **2023**, *13*, 2857. [CrossRef] [PubMed]
79. Abdullah, N.; Mohamed, A.R.; Ramli, M.Z.; Nor, N.M. Influence of Surface Characteristics of Palm Shell Activated Carbon Modified with Nanostructured Nickel for Reactive Adsorption of Hydrogen Sulfide. *J. Appl. Sci. Eng.* **2021**, *25*, 605–612.
80. Yoon, S.; Hassan, M.; Chung, Y. Multiscale Computational Modeling and Process Economic Optimization of All-Silica Zeolites for Adsorptive Separation of Ternary ($H_2S/CO_2/CH_4$) Gas Mixture. Available online: https://ssrn.com/abstract=4805277 (accessed on 23 December 2025).
81. Lin, Y.; Li, Y.; Xu, Z.; Guo, J.; Zhu, T. Carbon consumption and adsorption-regeneration of H_2S on activated carbon for coke oven flue gas purification. *Environ. Sci. Pollut. Res.* **2021**, *28*, 60557–60568. [CrossRef]
82. Spiridonova, E.A.; Samonin, V.V.; Podvyaznikov, M.L.; Morozova, V.Y. Production and research of Fullerene-Modified Chemical Adsorbent of Ammonia based on activated Carbon. *Russ. J. Appl. Chem.* **2020**, *93*, 691–697. [CrossRef]
83. Kerimkulova, A.R.; Azat, S.; Velasco, L.; Mansurov, Z.A.; Lodewyckx, P.; Tulepov, M.I.; Kerimkulova, M.R.; Berezovskaya, I.; Imangazy, A. Granular rice husk-based sorbents for sorption of vapors of organic and inorganic matters. *J. Chem. Technol. Metall.* **2019**, *54*, 578–584.
84. Zhang, C.; Shiu, W.-T.; Chang, L.-Y.; Chu, K.; Hu, P.; Adsetts, J.; Liu, L.; Zhang, Q.; Ding, Z. A Comparative Study of Band Structures and Quantum Confinement Effects in Graphene and Nitrogen-Doped Carbon Quantum Dot. *Can. J. Chem.* **2025**, *103*, 617–624. [CrossRef]
85. Arif, M.; Akram, I.; Umair, M.; Ghaffar, A.; Ghaffar, U.; Yaqoob, M.Z. Graphene Plasmonics and Its Technological Frontiers. *Kashf J. Multidiscip. Res.* **2025**, *2*, 87–101.
86. Tahsin, M.; Shahinuzzaman, M.; Akter, T.; Abdur, R.; Bashar, M.S.; Kadir, R.; Hoque, S.; Jamal, M.S.; Hossain, M. Improved CO_2 adsorption and desorption using chemically derived activated carbon from corn cob hard shell. *Carbon Trends* **2025**, *19*, 100495. [CrossRef]
87. Madagalam, M.; Bartoli, M.; Tagliaferro, A. A short overview on graphene and graphene-related materials for electrochemical gas sensing. *Materials* **2024**, *17*, 303. [CrossRef]
88. Gao, X.; Liu, S.; Zhang, Y.; Luo, Z.; Ni, M.; Cen, K. Adsorption and reduction of NO_2 over activated carbon at low temperature. *Fuel Process. Technol.* **2011**, *92*, 139–146. [CrossRef]
89. Li, B.; Ma, C. Study on the mechanism of SO_2 removal by activated carbon. *Energy Procedia* **2018**, *153*, 471–477. [CrossRef]
90. Shakor, Z.M.; Parsafard, N.; Al-Shafei, E. Adsorption and separation modeling of CO_2, hydrogen, and biogas: A mathematical review. *J. Mater. Sci.* **2025**, *60*, 6850–6876. [CrossRef]
91. Li, J.; Pang, L.; Cai, F.; Yuan, X.; Kong, F. Adsorption properties of Pd3-modified double-vacancy defect graphene toward SF6 decomposition products. *Sensors* **2020**, *20*, 4188. [CrossRef] [PubMed]
92. Zhou, X.-Y.; Zhou, J.-L.; Guo, R.; Liu, Y.-J.; Yu, Y.F.; Zhang, B.; Wu, Y.-W.; Zhao, L.; Lu, Q. Effect of flue gas components on the removal of cadmium pollutants by transition metal-modified activated carbon: Density functional theory and thermodynamic study. *Fuel* **2023**, *343*, 128011. [CrossRef]
93. Iwakami, S.; Yakushiji, S.; Ohba, T. Graphene Functionalization by O_2, H_2, and Ar Plasma Treatments for Improved NH_3 Gas Sensing. *ACS Appl. Mater. Interfaces* **2024**, *17*, 1992–1999. [CrossRef]
94. Melezhik, A.V.; Smolsky, G.V.; Zelenin, A.D.; Neskoromnaya, E.A.; Alekhina, O.V.; Burakov, A.E.; Tkachev, A.G. Synthesis of carbon materials with abnormally high specific surface area. *Adv. Mater. Technol.* **2019**, *2*, 19–24.
95. Ramezanzadeh, M.; Asghari, M.; Ramezanzadeh, B.; Bahlakeh, G. Fabrication of an efficient system for Zn ions removal from industrial wastewater based on graphene oxide nanosheets decorated with highly crystalline polyaniline nanofibers (GO-PANI): Experimental and ab initio quantum mechanics approaches. *Chem. Eng. J.* **2018**, *337*, 385–397. [CrossRef]
96. Khiem, T.N.; Chinh, H.D.; Van Tuan, P.; Tan, V.T. Adsorption capacities of reduced graphene oxide: Effect of reductants. *Mater. Res. Express* **2019**, *6*, 075615. [CrossRef]
97. Agrawal, P.S.; Belkhode, P.N.; Brijpuriya, D.S.; Gouda, S.P.; Rokhum, S.L. Stimulation in fullerene for adsorbing pollutant gases: A review. *Chem. Phys. Impact* **2023**, *6*, 100156. [CrossRef]
98. Haghgoo, S.; Nekoei, A.R. Metal oxide adsorption on fullerene C_{60} and its potential for adsorption of pollutant gases; density functional theory studies. *RSC Adv.* **2021**, *11*, 17377–17390. [CrossRef] [PubMed]

99. Mo, S.-C.; Qiu, X.-Y.; Nie, J.; Li, G.-Y.; Ning, F.; Chen, S.-Z. Long-range ordered porous carbon C52: A high-performance anode metallic material for next-generation Li-ion batteries with extremely high capacity. *J. Energy Storage* **2025**, *110*, 115286. [CrossRef]
100. Ahmer, M.F.; Uddin, M.K. A Review on Recent Developments in Polyindole–Based Nanocomposite Electrode Materials for Supercapacitor Applications. *Energy Storage* **2025**, *7*, e70168. [CrossRef]
101. Díez-Pascual, A.M. Carbon-based nanomaterials 4.0. *Int. J. Mol. Sci.* **2024**, *25*, 3032. [CrossRef] [PubMed]
102. Lagos, K.J.; Buzzá, H.H.; Bagnato, V.S.; Romero, M.P. Carbon-based materials in photodynamic and photothermal therapies applied to tumor destruction. *Int. J. Mol. Sci.* **2021**, *23*, 22. [CrossRef]
103. Lima, E.C.; Gomes, A.A.; Tran, H.N. Comparison of the nonlinear and linear forms of the van't Hoff equation for calculation of adsorption thermodynamic parameters (ΔS° and ΔH°). *J. Mol. Liq.* **2020**, *311*, 113315. [CrossRef]
104. John, J.P.; T.E., M.N.; T.K., B.S. A comprehensive review on the environmental applications of graphene–carbon nanotube hybrids: Recent progress, challenges and prospects. *Mater. Adv.* **2021**, *2*, 6816–6838. [CrossRef]
105. Abedi, M.; Fangueiro, R.; Correia, A.G. An effective method for hybrid CNT/GNP dispersion and its effects on the mechanical, microstructural, thermal, and electrical properties of multifunctional cementitious composites. *J. Nanomater.* **2020**, *2020*, 6749150. [CrossRef]
106. Etesami, M.; Nguyen, M.T.; Yonezawa, T.; Tuantranont, A.; Somwangthanaroj, A.; Kheawhom, S. 3D carbon nanotubes-graphene hybrids for energy conversion and storage applications. *Chem. Eng. J.* **2022**, *446*, 137190. [CrossRef]
107. Yousefi, K. Graphene-carbon nanotube hybrids: Synthesis and application. *J. Environ. Treat. Tech.* **2021**, *9*, 224–232.
108. Hsiao, S.-Y.; You, S.-W.; Wang, C.; Deng, J.-G.; Hsi, H.-C. Adsorption of volatile organic compounds and microwave regeneration on self-prepared high-surface-area beaded activated carbon. *Aerosol Air Qual. Res.* **2022**, *22*, 220010. [CrossRef]
109. Pazniak, H.; Plugin, I.A.; Loes, M.J.; Inerbaev, T.M.; Burmistrov, I.N.; Gorshenkov, M.; Polcak, J.; Varezhnikov, A.S.; Sommer, M.; Kuznetsov, D.V.; et al. Partially oxidized $Ti_3C_2T_x$ MXenes for fast and selective detection of organic vapors at part-per-million concentrations. *ACS Appl. Nano Mater.* **2020**, *3*, 3195–3204. [CrossRef]
110. Heinritzi, M.; Dada, L.; Simon, M.; Stolzenburg, D.; Wagner, A.C.; Fischer, L.; Ahonen, L.R.; Amanatidis, S.; Baalbaki, R.; Baccarini, A.; et al. Molecular understanding of the suppression of new-particle formation by isoprene. *Atmos. Chem. Phys.* **2020**, *20*, 11809–11821. [CrossRef]
111. Umair, M.; Ali, M.; Ismail, M.; Ali, E.; Basit, A.; Farooq, S.A.; Akhter, A.; Shabbir, A.; Qurban, M.H. Revolutionizing Energy Storage: Unleashing the Power of Carbon Nanotubes in Next-Gen Batteries and Advanced Materials Science. *Sch. Int. J. Chem. Mater. Sci.* **2025**, *8*, 77–90. [CrossRef]
112. Sengupta, J.; Hussain, C.M. Carbon Nanotube-Based Field-Effect Transistor Biosensors for Biomedical Applications: Decadal Developments and Advancements (2016–2025). *Biosensors* **2025**, *15*, 296. [CrossRef] [PubMed]
113. Pyo, S.; Eun, Y.; Sim, J.; Kim, K.; Choi, J. Carbon nanotube-graphene hybrids for soft electronics, sensors, and actuators. *Micro Nano Syst. Lett.* **2022**, *10*, 9. [CrossRef]
114. Hong, Z.; Zheng, Z.; Kong, L.; Zhao, L.; Liu, S.; Li, W.; Shi, J. Welded carbon nanotube–graphene hybrids with tunable strain sensing behavior for wide-range bio-signal monitoring. *Polymers* **2024**, *16*, 238. [CrossRef]
115. Xiao, Y.; Luo, F.; Zhang, Y.; Hu, F.; Zhu, M.; Qin, S. A review on graphene-based nano-electromechanical resonators: Fabrication, performance, and applications. *Micromachines* **2022**, *13*, 215. [CrossRef] [PubMed]
116. Ajori, S.; Sadeghi, F. Design of high-frequency carbon nanotube–carbon nanotorus oscillators for energy harvesting: A molecular dynamics study. *Langmuir* **2024**, *40*, 4811–4823. [CrossRef]
117. Kao, H.-L.; Chang, L.-C.; Tsai, Y.-C.; Chiu, H.-C. Microwave gas sensor based on carbon nanotubes loaded on open loop ring resonators. *IEEE Electron Device Lett.* **2022**, *43*, 1740–1743. [CrossRef]
118. Shah, M.A.; Pirzada, B.M.; Price, G.; Shibiru, A.L.; Qurashi, A. Applications of nanotechnology in smart textile industry: A critical review. *J. Adv. Res.* **2022**, *38*, 55–75. [CrossRef] [PubMed]
119. Shaheen, T.I. Nanotechnology for modern textiles: Highlights on smart applications. *J. Text. Inst.* **2022**, *113*, 2274–2284. [CrossRef]
120. Syduzzaman, M.; Hassan, A.; Anik, H.R.; Akter, M.; Islam, M.R. Nanotechnology for high-performance textiles: A promising frontier for innovation. *ChemNanoMat* **2023**, *9*, e202300205. [CrossRef]
121. Sun, D.; Ahmad, M.; Siddiqui, M.O.R.; Iqbal, K. Nanotechnology in smart textiles. In *Nanotechnology in Textile Finishing: Advancements and Applications*; Springer Nature: Singapore, 2024; pp. 441–459.
122. Mondal, M.I.H.; Rahman, N.; Pervez, M.N.; Islam, M.K.; Habib, M.A.; Ahmed, F. Nanotechnology for smart textiles—Recent development and applications. In *Smart Textiles from Natural Resources*; Woodhead Publishing: Cambridge, UK, 2024; pp. 143–187.
123. Schmaltz, T.; Wormer, L.; Schmoch, U.; Döscher, H. Graphene roadmap briefs (No. 3): Meta-market analysis 2023. *2D Mater.* **2024**, *11*, 022002. [CrossRef]
124. Döscher, H.; Schmaltz, T.; Neef, C.; Thielmann, A.; Reiss, T. Graphene Roadmap Briefs (No. 2): Industrialization status and prospects 2020. *2D Mater.* **2021**, *8*, 022005. [CrossRef]
125. Munuera, J.; Britnell, L.; Santoro, C.; Cuéllar-Franca, R.; Casiraghi, C. A review on sustainable production of graphene and related life cycle assessment. *2D Mater.* **2021**, *9*, 012002. [CrossRef]

126. Al Faruque, A.; Syduzzaman, M.; Sarkar, J.; Bilisik, K.; Naebe, M. A review on the production methods and applications of graphene-based materials. *Nanomaterials* **2021**, *11*, 2414. [CrossRef] [PubMed]
127. Ali, M.A.; Irfan, M.S.; Khan, T.; Khalid, M.Y.; Umer, R. Graphene nanoparticles as data generating digital materials in industry 4.0. *Sci. Rep.* **2023**, *13*, 4945. [CrossRef] [PubMed]
128. Dai, H.; Wang, J. Advances in Catalytic Oxidation of Methane and Carbon Monoxide. *Catalysts* **2024**, *14*, 642. [CrossRef]
129. Florent, M.; Bandosz, T.J. Surfactant-modified biosolid-derived materials as efficient H_2S removal media: Synergistic effects of carbon phase properties and inorganic phase chemistry on reactive adsorption. *Chem. Eng. J.* **2020**, *401*, 125986. [CrossRef]
130. Busca, G.; Spennati, E.; Riani, P.; Garbarino, G. Looking for an optimal composition of nickel-based catalysts for CO_2 methanation. *Energies* **2023**, *16*, 5304. [CrossRef]
131. Promhuad, P.; Sawatmongkhon, B.; Wongchang, T.; Sukjit, E.; Theinnoi, N.; Theinnoi, K. Silver-Based Catalysts on Metal Oxides for Diesel Particulate Matter Oxidation: Insights from In Situ DRIFTS. *ChemEngineering* **2025**, *9*, 42. [CrossRef]
132. Martin, A.; Kalevaru, V.N.; Radnik, J. Palladium in Heterogeneous Oxidation Catalysis. In *Petrochemical Catalyst Materials, Processes, and Emerging Technologies*; IGI Global Scientific Publishing: New York, NY, USA, 2016; pp. 53–81.